AD 257 807

WADD TECHNICAL REPORT 60-892

THE DOWNSTREAM INFLUENCE OF MASS TRANSFER AT THE NOSE OF A SLENDER CONE

by

Robert J. Cresci and Paul A. Libby

MAY 1961

XEROX

POLYTECHNIC INSTITUTE OF BROOKLYN

DEPARTMENT
of
AEROSPACE ENGINEERING
and
APPLIED MECHANICS

PIBAL REPORT NO. 634

NOTICES

When Government drawings, specifications, or other data are used for any purpose other than in connection with a definitely related Government procurement operation, the United States Government thereby incurs no responsibility nor any obligation whatsoever; the fact that the Government may have formulated, furnished, or in any way supplied the said drawings, specifications, or other data, is not to be regarded by implication or otherwise as in any manner licensing the holder or any other person or corporation, or conveying any rights or permission to manufacture, use, or sell any patented invention that may in any way be related thereto.

The information furnished herewith is made available for study upon the understanding that Polytechnic Institute of Brooklyn proprietary interest in and relating thereto shall not be impaired.

Qualified requesters may obtain copies of this report from the Armed Services Technical Information Agency, (ASTIA), Arlington Hall Station, Arlington 12, Virginia.

This report has been released to the Offices of Technical Services, U.S. Department of Commerce, Washington 25, D. C. for sale to the general public.

Copies of ARL Technical Reports and Technical Notes should not be returned to the Aeronautical Research Laboratories unless return is required by security considerations, contractual obligations, or notices on a specific document.

WADD TECHNICAL REPORT 60-892

THE DOWNSTREAM INFLUENCE OF MASS TRANSFER AT THE NOSE OF A SLENDER CONE

Robert J. Cresci
Paul A. Libby

Polytechnic Institute of Brooklyn

MAY 1961

Materials Central
Contract No. AF 33(616)-5944
Project No. 7364

Aeronautical Research Laboratory
Contract No. AF 33(616)-7661
Project No. 7064

Aeronautical Systems Division
Air Force Systems Command
United States Air Force
Wright-Patterson Air Force Base, Ohio

FOREWORD

This report was prepared by the Polytechnic Institute of Brooklyn under two contracts. The experimental work and data reduction were performed under USAF Contract AF 33(616)-5944; the theoretical analysis, interpretation of the data, and preparation of the report were performed under USAF Contract AF 33(616)-7661. The contracts were initiated under Project No. 7364, "Experimental Techniques for Materials Research," Task No. 73652, "Intense Thermal Energy Transfer Into Materials," and Project No. 7064, "Research on Aerodynamic Flow Fields," Task No. 70169, "Thermal-Aerodynamic Characteristics at Hypersonic Mach Numbers," respectively. The work was administered by the Materials Central, Deputy of Advanced Systems Technology, Aeronautical Systems Division and the Aeronautical Research Laboratory, Air Force Office of Aerospace Research, with Mr. Hyman Marcus and Lt. John D. Anderson acting as project engineers, respectively.

The report covers work conducted from February 1960 to February 1961.

This report was prepared by Dr. Robert J. Cresci, Research Assistant Professor of Aeronautical Engineering and Dr. Paul A. Libby, Professor of Aeronautical Engineering and Assistant Director of the Aerodynamics Laboratory.

The authors are pleased to acknowledge the valuable assistance of the hypersonic and computing staffs of PIBAL in carrying out this research, and of Professor Lu Ting for suggestions concerning the analysis of the shock stand-off distance.

ABSTRACT

The influence of localized mass transfer at the nose of a slender cone under hypersonic flow conditions has been studied by experimental and theoretical means. Two gaseous coolants, nitrogen and helium are injected through a porous plug subtending a half angle of 30°. The effect of the mass transfer on the shock shape, pressure distribution, heat transfer and transition are investigated. The experimental work involved tests in the Mach number 8.0 tunnel at PIBAL. The theoretical analysis involved a study of the effect of mass transfer on the shock stand-off distance and leads to an inviscid flow parameter permitting the experimentally determined shock shape and pressure distribution to be extrapolated to other than test conditions and to other coolant gases. There is obtained the maximum value of this parameter resulting in no significant alteration of the pressure distribution on the cone and thus defining the flows in which boundary layer type of similarity applies.

Significant reductions in heat transfer are obtained with injection. Indeed with small amounts of helium injection the peak heating is found to occur downstream on the cone and to be an order of magnitude less than would occur at the stagnation point without mass transfer. With nitrogen early transition is found to occur so that local heating rates are actually increased over those prevailing at the same Reynolds number without injection.

PUBLICATION REVIEW

This report has been reviewed and is approved.

FOR THE COMMANDER:

JULES I. WITTEBORT
Chief, Thermophysics Branch
Physics Laboratory
Materials Central

TABLE OF CONTENTS

LIST OF FIGURES

LIST OF FIGURES (Contd)

LIST OF SYMBOLS

c_p	specific heat at constant pressure
h	enthalpy
$\bar{h}$	$= h/h_{s_e}$, static enthalpy ratio
k	thermal conductivity
K	density ratio across the bow shock wave
m_c	mass flow of injected gas per unit time
N_{Nu}	$= qR_o(c_p)_{s_e}/(h_{s_e}-h_w)k_{s_e}$, Nusselt number
$\tilde{N}_R$	$= (\rho_{s_e}\sqrt{h_{s_e}}R_o/\mu_{s_e})\varphi_{s_e}^{\frac{1}{2}}$, Reynolds number
N_1	$= (m_c/R_o\mu_{s_e})\tilde{N}_R^{-\frac{1}{2}}$, mass transfer similarity parameter
N_2	$= N_{Nu}\tilde{N}_R^{-\frac{1}{2}}$, heat transfer similarity parameter
N_s	$= m_c R_o^{-2}(\theta_w W_e)^{\frac{1}{2}}(\rho_{s_e}\rho_{s_e}W_c)^{-\frac{1}{2}}$, inviscid flow parameter
p	pressure
q	surface heat transfer rate.
r	radial coordinate measured from the center of the spherical nose
$\bar{r}$	ratio of radial coordinate to interface radius
r_o	radius of interface
r_s	shock radius
$\bar{r}_s$	ratio of shock to interface radius
R_o	nondimensionalizing length (spherical nose radius)
$\bar{R}_o$	ratio of body to interface radius
u	velocity component parallel to the surface
$\bar{u}$	$= u_e/\sqrt{h_{s_e}}$, nondimensionalized velocity parallel to the surface
v	velocity component normal to the surface

V_∞	free stream velocity
W	molecular weight
x	space coordinate along the surface
$\bar{x}$	$= x/R_o$, nondimensionalized space coordinate along the surface
β_e	$= du_e/dx$, velocity gradient of external flow
Δ	shock stand-off distance
θ	$= T/T_{s_e}$, temperature ratio
μ	viscosity coefficient
$\bar{\mu}$	$= \mu_e/\mu_{s_e}$, viscosity ratio
ρ	mass density
$\bar{\rho}$	$= \rho_e/\rho_{s_e}$, density ratio
$\dot{\Phi}_{s_e}$	$\equiv p_{s_e}/\rho_{s_e} h_{s_e}$, real gas parameter
Ψ	stream function defined by equations (I-2) and (I-3)
ω	vorticity defined by equation (I-4)

Subscripts

c	denotes foreign gas characteristics prior to injection
e	denotes local conditions external to the boundary layer.
i	denotes termination of injection region
s_e	denotes conditions external to the boundary layer at the stagnation point
w	denotes conditions evaluated at the wall

I - INTRODUCTION

The use of mass transfer for the reduction of heat transfer has been the subject of considerable research in connection with high performance propulsion systems and with hypersonic flight. As a result a variety of heat protection systems, some involving mass transfer have been developed.

The research reported herein pertains to the use of localized mass transfer for the reduction of heat transfer in the nose region and on the downstream conical portion of a slender cone. The system considered is shown schematically in Figure 1a. A relatively slender cone has a spherical nose made of a porous material through which a gaseous coolant is injected. The coolant has two effects on the heat transfer; it reduces and absorbs the heat transferred to the spherical region and reduces the heat transferred to the downstream conical portion of the body. In addition, the coolant can alter the shock shape and the pressure distribution on the body.

This localized mass transfer system is conceptually similar to the system studied in reference 1. There a hemisphere cylinder with a porous plug subtending an angle of roughly 10° with the axis of symmetry was considered. The gaseous coolant injected through the plug reduced the heat transfer at the stagnation point and on the downstream portion of the hemisphere. The coolants tested were helium, nitrogen, argon and krypton.

In considering the similarity conditions for these localized mass transfer systems the present authors in reference 1 distinguish between two types of flows; those in which the coolant is introduced into a classical boundary layer without significant alteration of the inviscid flow as shown in Figure 1b, and those in which the entire flow field is influenced by the coolant flow as shown in Figure 1c. For the first type of flow, similarity conditions based on the boundary layer equations are applicable and can be employed to extrapolate test data to other Reynolds numbers and to other Mach numbers if the pressure distribution is Mach number insensitive. On the other hand, flows of the second type lead to stringent similitude requirements; indeed, no extrapolation of test data to other Reynolds and Mach numbers is, in general, possible. These flows involve viscous layers which are relatively thick compared to the shock layer and to the cylindrical radius. Consequently, the shock shape and pressure distribution change as either the rate of mass transfer, or the Reynolds number, or the Mach number is changed.

The experimental results in reference 1 indicated that for the porous material, flow conditions, and rates of coolant mass flow employed therein, the boundary layer was laminar and the inviscid flow field was essentially unaltered at even the highest rates of mass transfer; therefore

---

Manuscript released February 1961 for publication as a WADD Technical Report.

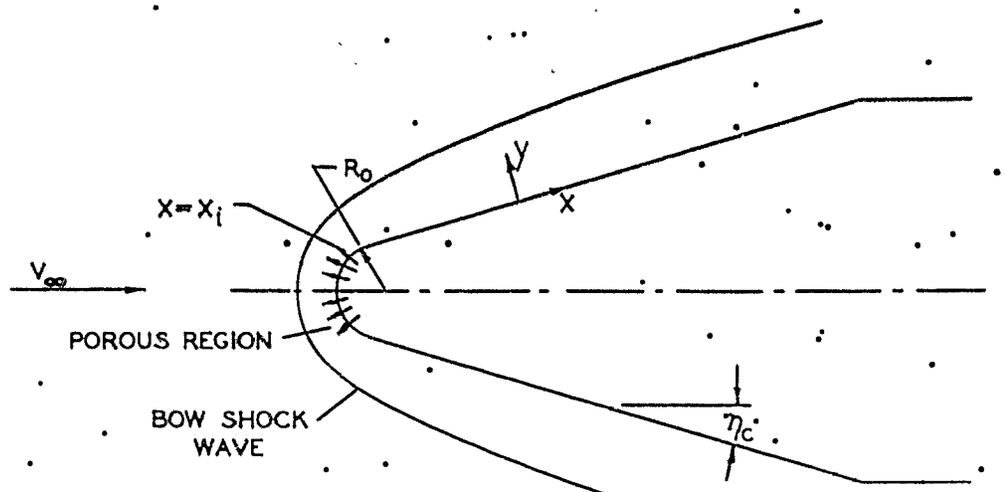

(a) COORDINATE SYSTEM AND GEOMETRY

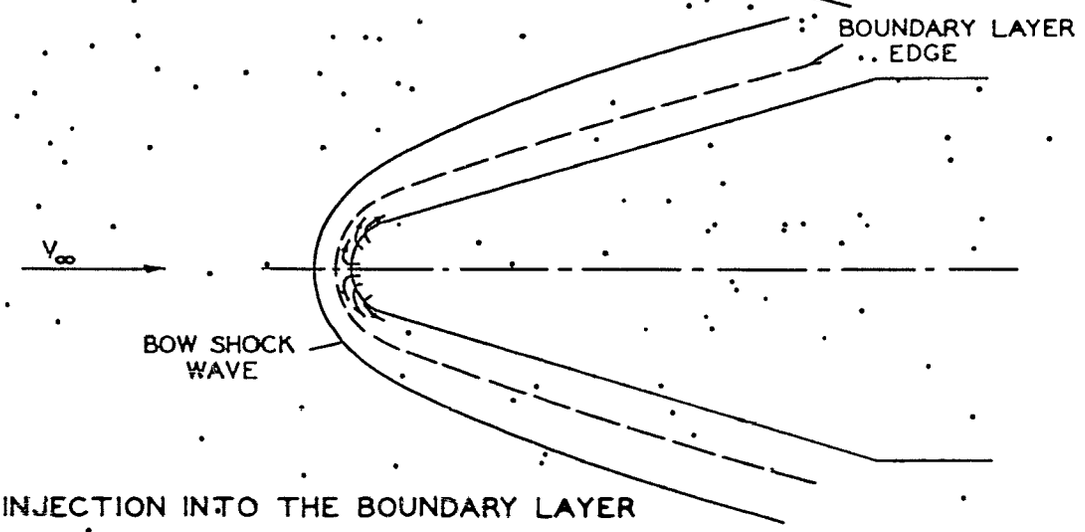

(b) INJECTION INTO THE BOUNDARY LAYER

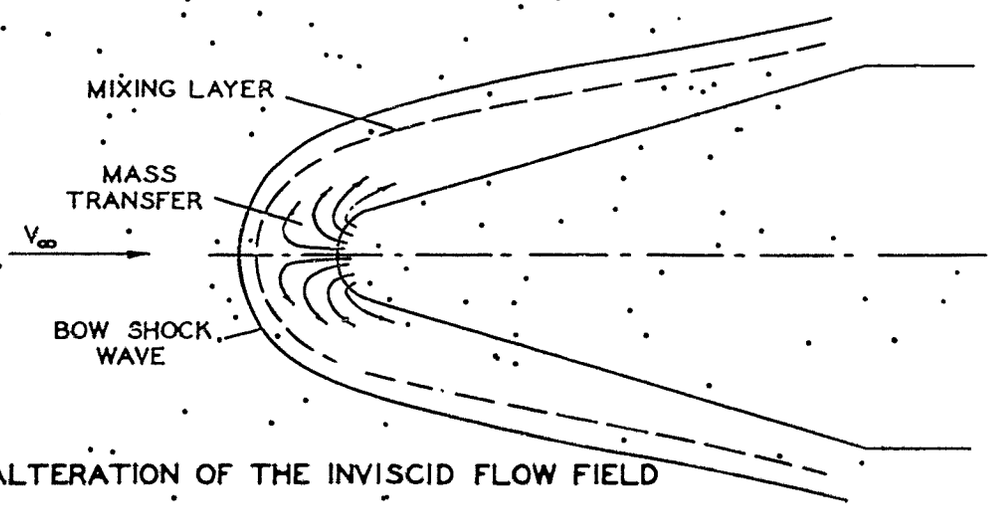

(c) ALTERATION OF THE INVISCID FLOW FIELD

FIG.(1) SCHEMATIC DIAGRAM OF THE MASS TRANSFER SYSTEM

the flow was of the first type. Accordingly, the similarity parameters developed in reference 1 could be used to extrapolate the test results either to flight or to other test conditions provided, of course, that the flow remains laminar.

For the localized mass transfer system discussed herein the same considerations with respect to flow similarity will apply. For sufficiently low rates of coolant flow, the inviscid flow field will be unaltered by the injection and similarity parameters presented in reference 1 are applicable as follows: Consider two geometrically similar bodies as shown schematically in Figure 1a, with identical inviscid flows in terms of the distribution of $\bar{\rho} = \bar{\rho}(\bar{x})$, $\bar{u} = \bar{u}(\bar{x})$, etc. Assume that the chemical compositions of the coolant and of the external gas stream are fixed and equal in the flows. Assume further that the enthalpy ratio h_c (coolant-to-free-stream stagnation) and the distribution of temperature ratio θ_w (wall-to-free-stream stagnation) are the same in the two flows. Then the rates of laminar heat transfer to the impermeable surface on the two bodies are related by the similarity parameters

$$N_2 = N_2(N_1, h_c, \theta_w, \bar{x}) \tag{1}$$

where N_1 and N_2 are respectively mass and heat transfer parameters defined as follows:

$$N_1 \equiv m_c / R_o \mu_{s_e} \tilde{N}_R^{\frac{1}{2}} \tag{2}$$

and

$$N_2 \equiv N_{Nu} / \tilde{N}_R^{\frac{1}{2}}$$

$$= [qR_o(c_p)_{s_e} / (h_{s_e} - h_w) k_{s_e}] [(\rho_{s_e} h_{s_e}^{\frac{1}{2}} R_o / \mu_{s_e})(p_{s_e} / \rho_{s_e} h_{s_e})^{\frac{1}{2}}]^{-\frac{1}{2}} \tag{3}$$

This result clearly permits heat transfer data obtained at one Reynolds number (N_R) to be extrapolated to other flow conditions provided N_1, h_c, θ_w and $\bar{x}_i$ are unaltered.

Consider the theoretical determination of the boundary layer characteristics of flows covered by these similarity requirements. If such a determination were possible, the functional relation expressed by Eq. (1) could be evaluated by theoretical analysis. Two regions along the surface can be identified; for $\bar{x} < \bar{x}_i$ the boundary layer involves mass transfer, while for $\bar{x} > \bar{x}_i$ the surface is impermeable. Now it was found in reference 1 that the rates of injection required to obtain a significant downstream effect from stagnation point mass transfer were considerably higher than those required to reduce substantially the heat transfer to the

porous surface itself. Indeed, the values of mass transfer per unit area per unit time $(\rho v)_w$ employed in those experiments were found to be up to 20 or 30 times those usually considered in theoretical analyses of transpiration cooling. It would be expected a priori that similarly high rates of mass transfer would be required in the configuration considered here for essential reductions in the heat transfer to the downstream conical section.

In reference 2 a theoretical analysis of the stagnation point boundary layer with large rates of air-to-air injection was carried out. It was found that the boundary layers could be characterized by an isothermal shear layer close to the surface and a relatively thin mixing zone adjusting this inner flow to the external flow values. This result suggested an integral method which was shown to lead to accurate values for the gross boundary layer properties. * This characterization of the stagnation point boundary layer also suggests the idealization which will be employed herein for the study of the alteration of shock stand-off distance with injection; accordingly, the boundary layer is replaced by an isothermal shear layer which is matched to the external flow by a slip surface.

It appears then that the analysis of the first region $(0 < \bar{x} < \bar{x}_i)$ for large rates of injection can be carried out according to either of two approximate methods. The stagnation point analysis for large rates of injection can be considered to apply approximately over the entire range of $\bar{x}$. In general, the requirements of boundary layer similarity, especially with respect to the distribution of the rate of mass transfer, will not be exactly satisfied; however, a stagnation point analysis should be sufficiently accurate for most purposes. A second method of analysis would be to apply an integral method as in reference 2 to the development of the boundary layer over the entire range of $\bar{x}$ starting with stagnation point values.

The analysis of the boundary layer in the downstream impermeable region $(\bar{x} \geq \bar{x}_i)$ requires the treatment of the initial value problem of boundary layer theory. At $\bar{x} = \bar{x}_i$ the velocity, stagnation enthalpy and concentration profiles are given by the analysis of the porous region; the downstream development of the boundary layer is desired. This problem can be treated by integral methods as in references 3 and 4, by finite difference methods as in reference 5, or by the method of "strips", recently published by Pallone (reference 6) and more recently described by Dorodnitsyn. **

---

*The analysis of reference 2 is at present being extended to the case of helium-to-air injection.

**At the Second International Conference of the Aeronautical Sciences, Zurich, Switzerland, September 11-16, 1960.

In this report there are presented the results of an experimental investigation of a configuration close to that shown schematically in Figure 1a. The tests were carried out at a Mach number of 8.0 in the hypersonic facility of PIBAL (cf. references 7 and 8). Two coolants, helium and nitrogen, were injected over sufficiently wide ranges of mass rates and Reynolds numbers, such that both types of flow described herein prevailed.

Three types of information were obtained from these tests; the first pertains to the alteration of the shock shape and pressure distribution by the injection. A theoretical analysis of the influence of mass transfer on the shock stand-off distance is carried out and shown to yield results in good agreement with experiment. The well-known approximations of a spherical shock with a constant density shock-layer are employed along with an idealization of an inner layer formed by the injected fluid; namely, an isothermal shear layer with vorticity. This theoretical model, which is applicable to both nitrogen and helium injection, suggests a combination of N_1 and N_R, i.e., a new inviscid flow parameter N_3. From the available pressure data, the maximum value of N_3 for no alteration in pressure distribution is obtained.

The second type of data presented in the report is the heat transfer to the downstream conical surface. Laminar, transitional and turbulent heat transfer rates are obtained and compared to the available theories for zero mass transfer. Significant reductions in laminar heat transfer result from the mass transfer but earlier transition is found to occur.

Finally, the third type of data presents the alteration of transition behavior with Reynolds number and mass transfer. These data are limited; additional tests would be required for reasonable knowledge of transition behavior.

II. MODEL DESIGN, TEST PROCEDURES AND TEST CONDITIONS

The model used in the tests is a blunt-nosed cone with a semi-vertex angle of 20°. The injection region, consisting of a spherically shaped porous cap, extends over a half angle of 30°. The details of the model design are shown in Figure 2 along with the the thermocouple and pressure tap locations. Figure 3 presents photographs of the model on the support prior to installation in the wind tunnel.

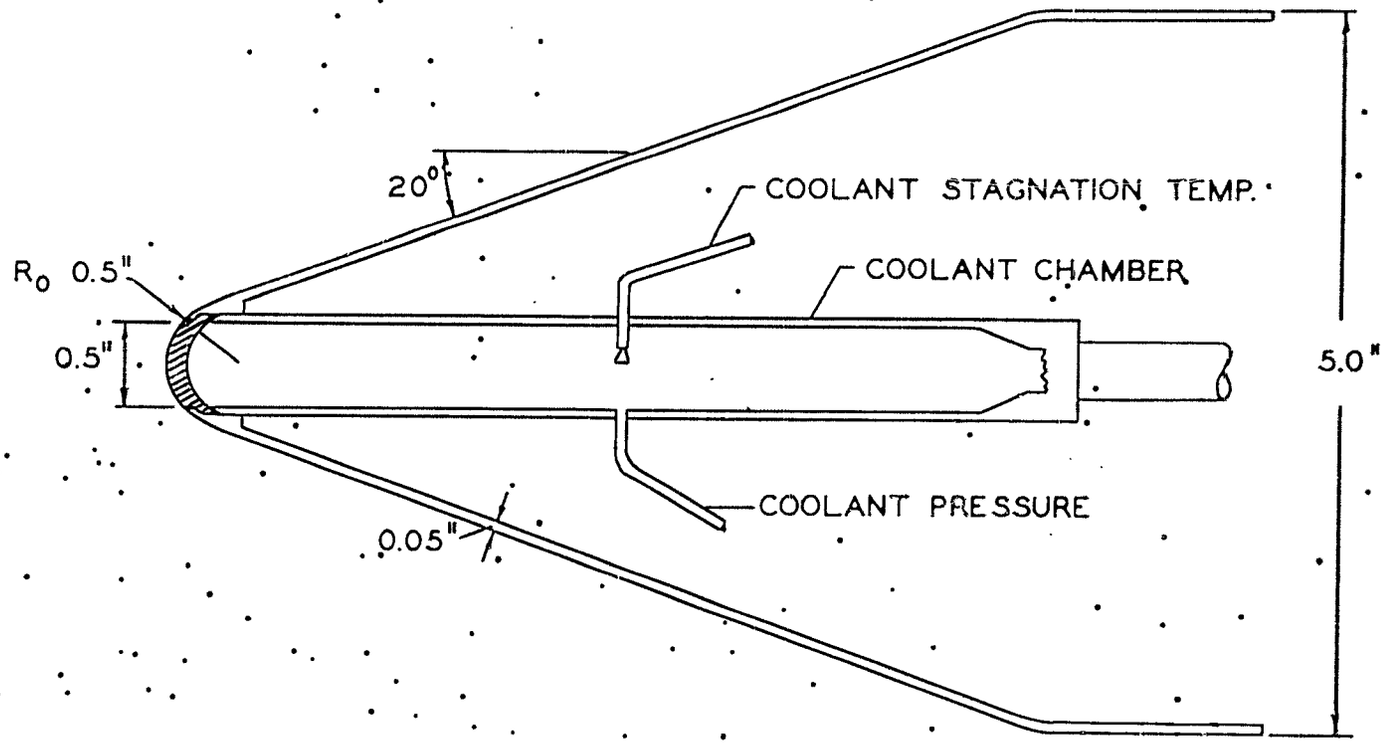

$\bar{X} = X/R_0$	1.85	2.84	3.85	4.84	5.84	6.85	7.84	8.85	9.84	10.84	11.84	12.84	13.25	13.75
THERMOCOUPLE #	1	2	3	4	5	6	7	8	9	10	11	12	13	
PRESSURE TAP #	1	2	3	4	5	6	7	8	9	10	11	12	13	14

FIG. (2) DETAILS OF MODEL DESIGN AND INSTRUMENTATION

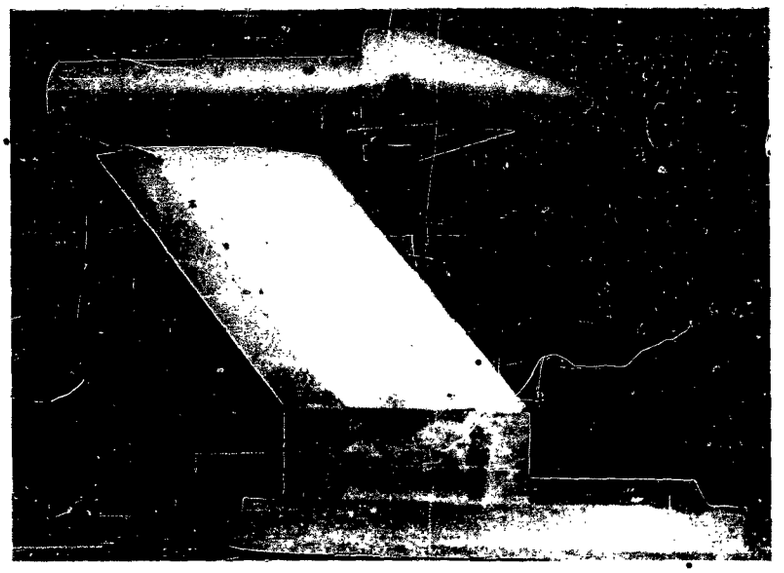

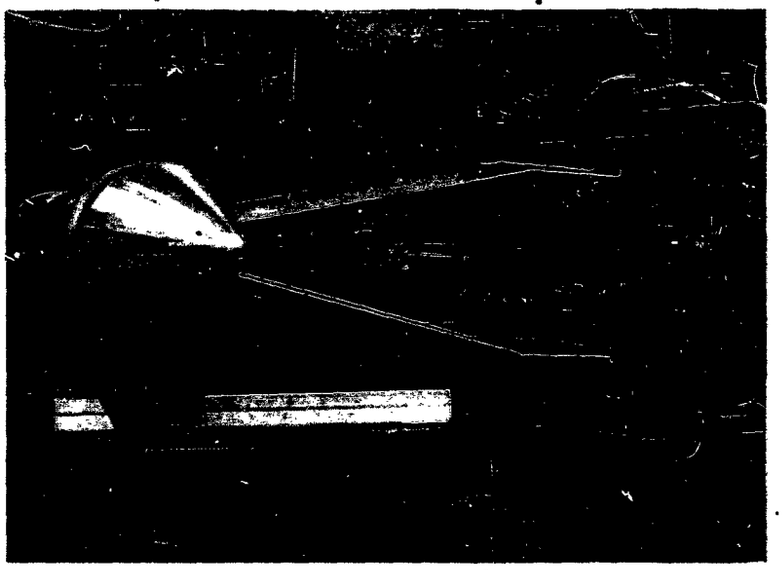

FIG.(3) PHOTOGRAPHS OF MODEL AND SUPPORT.

The wind tunnel tests presented herein were performed at a Mach number of 8.0, at a stagnation temperature of approximately 1700°R, and at free stream stagnation pressures varying between 150 and 600 psia. Schlieren pictures were taken during each test. The maximum mass flow injected at the model nose was 0.01 lb/sec. for helium and 0.03 lb/sec. for nitrogen. In terms of the nondimensional similarity parameters defined in the Introduction, the Reynolds number variation corresponds to $0.7 < \bar{N}_R \times 10^{-4} < 2.5$, and the mass transfer parameter variation $N_1 \leq 74$ for helium and $N_1 \leq 213$ for nitrogen. The coolant temperature remained essentially constant for all tests and was approximately 530°R. On the impermeable surface downstream of the injection region, the average wall temperature was 560°R for all the tests; thus, the heat transfer data correspond to an isothermal surface with $\theta_w \simeq 0.33$. The model was initially polished to a surface roughness of less than 4 micro-inches. As the test series proceeded, surface erosion occurred; however, the model surface was repolished so that the maximum roughness is believed to be in the neighborhood of 30 to 40μ for all tests.

Pressure data were obtained by differential transducers and recorded on single channel recording potentiometers. In order to minimize the response time, the reference chamber of the transducers was evacuated to a pressure slightly below the static pressure in the tunnel during the run. With this technique the steady state indication of pressure was achieved in about 5 seconds, permitting relatively short running times.

The heat transfer data were obtained by a transient technique utilizing a thin skinned model at an essentially uniform initial temperature. The local heat transfer rate can be related to the initial timewise derivative of the surface temperature; the details of the analysis and the method of thermocouple installation are discussed in detail in references 1 and 9, for example.

The mass transfer rate through the porous plug was determined by two independent measurements. A flow meter in the coolant supply line provided a direct measurement of the coolant flow; the measured pressure drop across the plug also determines the mass flow rate according to the following relation:

$$\dot{m}_c = C W_c^{0.55} [p_c^2 - p_s^2]^{0.55} \qquad (4)$$

The constant, C, was obtained by calibrating the porous plug over the entire mass flow range prior to installation in the tunnel. The mass transfer rates as determined by the two measurements differed by a maximum of 10% in all tests.* Coolant temperature was measured by an

*It is of interest to note that for the particular porous material used in these tests $p_c^2 >> p_s^2$ so that m_c is essentially constant with x. Thus the agreement between the calibrations with zero and hypersonic free stream velocity is not surprising.

open tip thermocouple located along the coolant chamber centerline.

The porous cap was formed by coining a flat sheet of porous stainless steel. Initially, the mean pore opening was 65 microns; however, as a result of the forming process the openings on the outer surface increased slightly. To ascertain qualitatively the effect this would have on the distribution of injection velocity, the spray pattern with water as a coolant was observed. Various plugs were tested until one was obtained with a relatively uniform spray distribution.

The accuracy of the measurements is estimated to be as follows: the overall error in the pressures on the cone surface is ± .02 psi. The mass flow of the coolant gas is in error by a maximum of ± 5% over the entire flow range. The heat transfer results involve many parameters affecting the final data; an overall estimate of the error is believed to be ± 10% in terms of the Nusselt number.

III. PRESENTATION AND DISCUSSION OF RESULTS

The data obtained in the tests present three different effects of the mass transfer; on the pressure distribution and shock shape, on the heat transfer to the cone, and on transition. The data pertaining thereto are discussed in the following sections.

Pressure Distribution and Shock Shape

Figures 4a-4c and 5a-5d present, respectively, the pressure data and typical schlieren photographs. In Figure 4a the pressure distribution for zero mass flow is presented as a line representing the mean of the data points. Also shown is the theoretically predicted pressure distribution for $M_\infty = 8.0$ with $T_s = 5000^\circ R$ obtained from reference 10, and the sharp cone value for a calorically perfect gas from reference 11, for example. The data points shown in Figure 4a along with the values of N_1 and $\tilde{N}_R$ pertaining thereto correspond to no alteration of the pressure distribution within experimental accuracy. In Figures 4b and 4c there are shown the pressure distributions which result from relatively large rates of nitrogen and helium injection, respectively. Again the values of N_1 and $\tilde{N}_R$ for each distribution are given.

From these figures and additional schlieren photographs the following observations may be made:

1) The experimentally determined pressure distribution over the entire cone, for zero mass transfer is within 10% of that theoretically

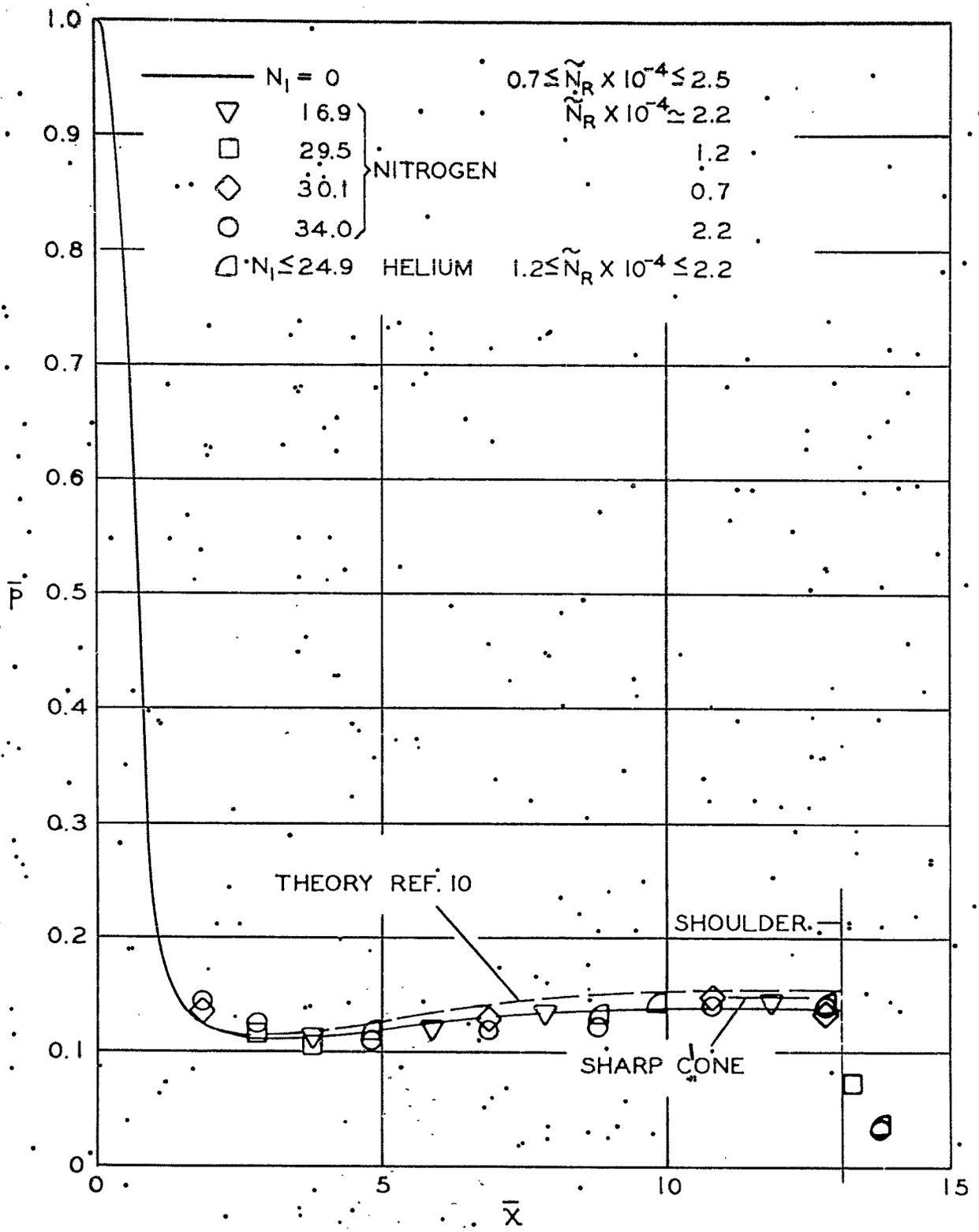

FIG. (4) PRESSURE DISTRIBUTION (a) NO ALTERATION DUE TO INJECTION

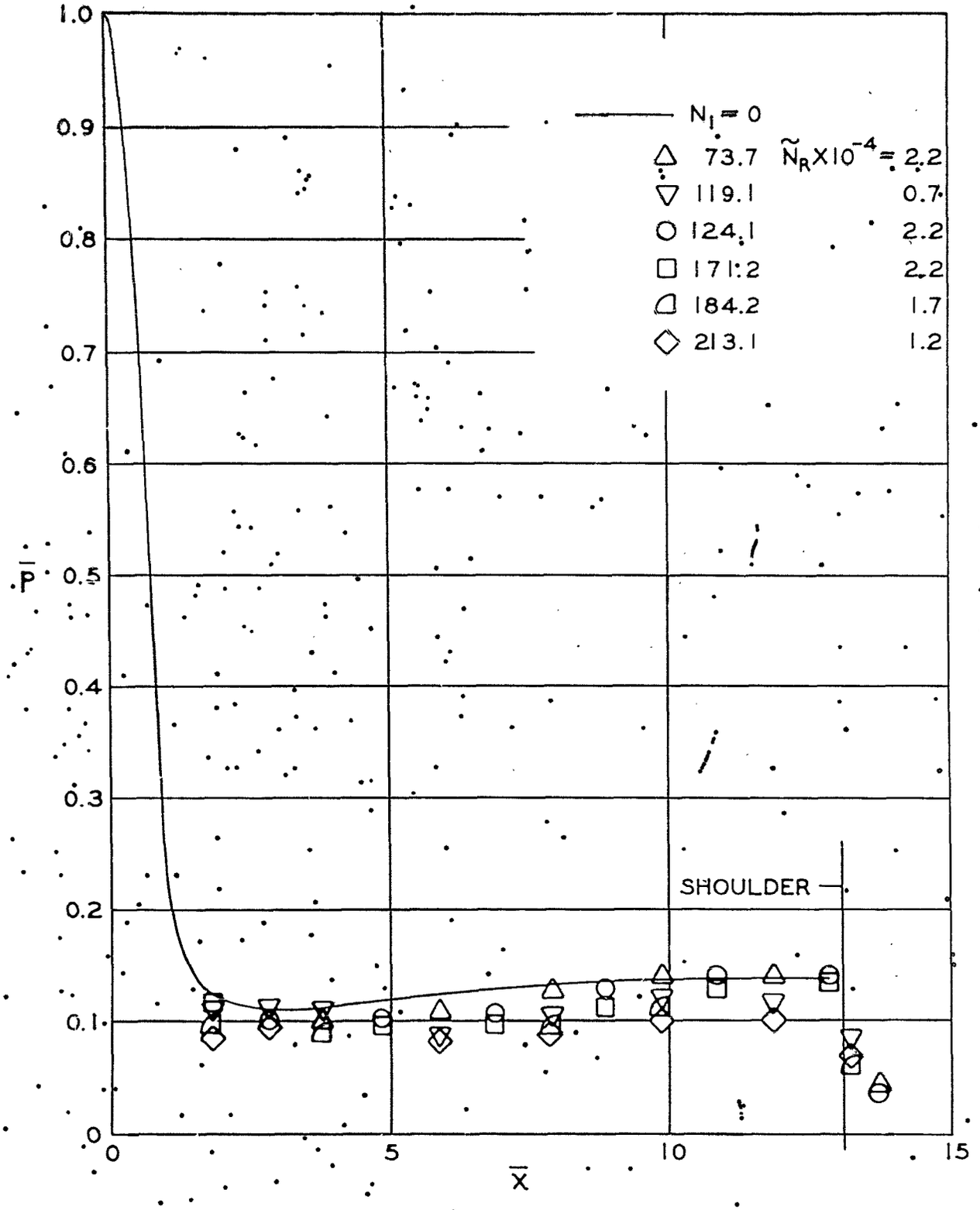

FIG. (4) PRESSURE DISTRIBUTION (b) NITROGEN INJECTION

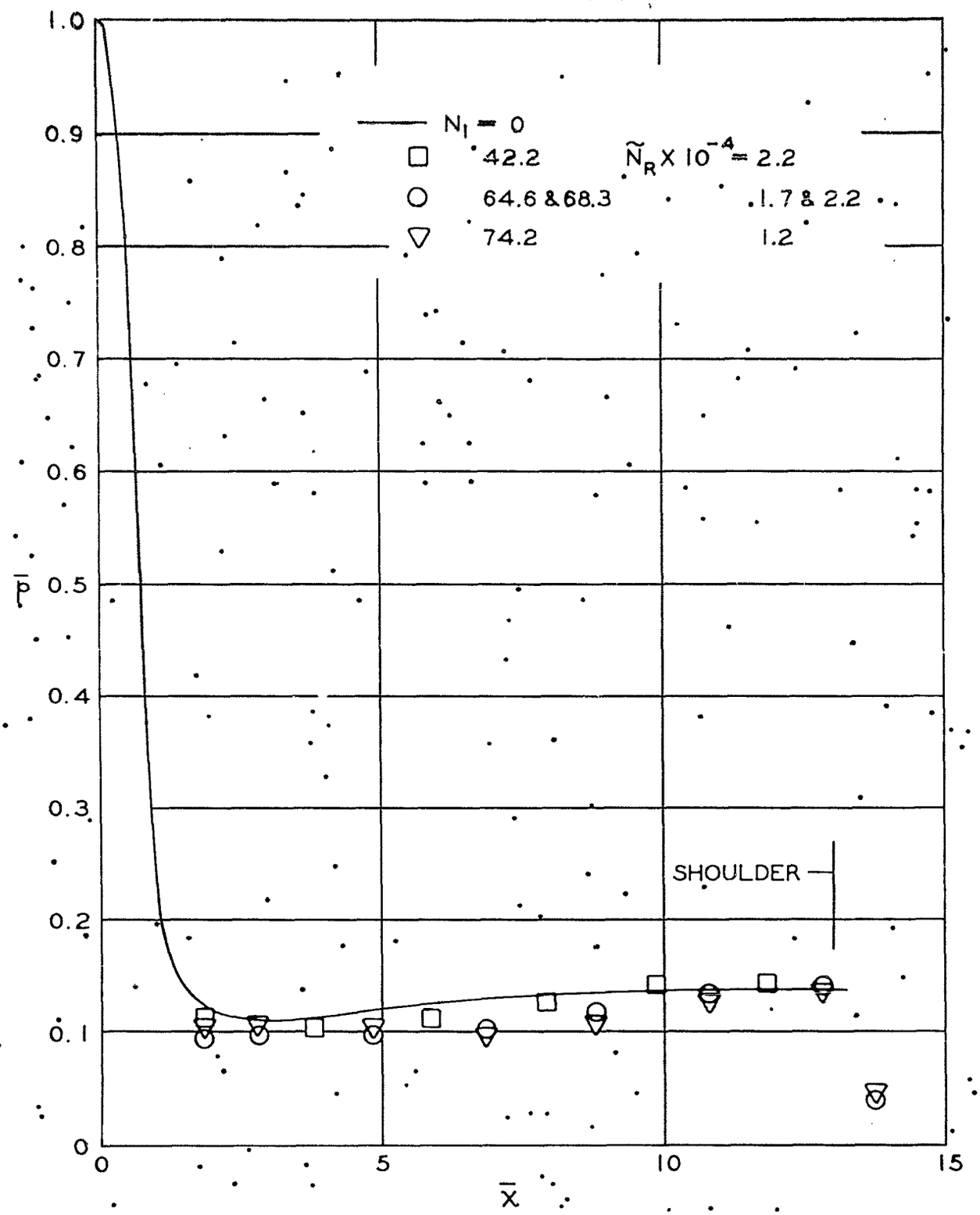

FIG. (4) PRESSURE DISTRIBUTION (c) HELIUM INJECTION

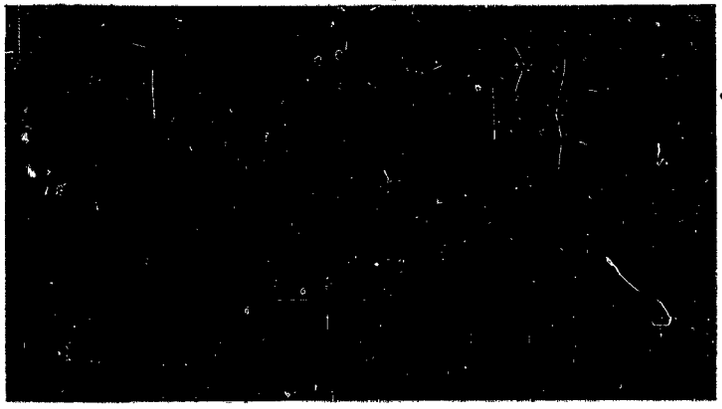

(a) $N_1 = 0$

(b) HELIUM; $N_1 = 24.9$, $N_3 = .278$

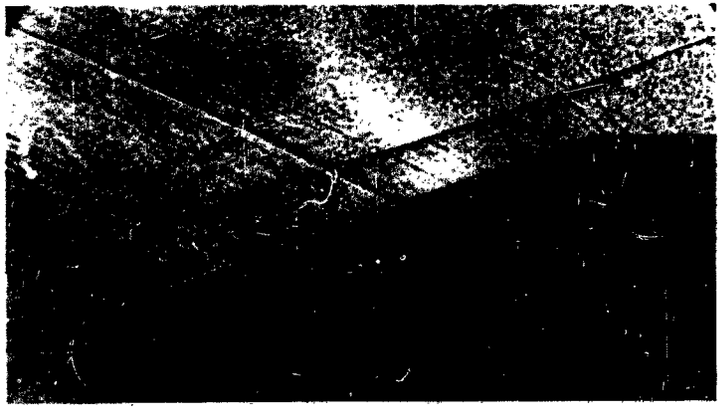

(c) NITROGEN, $N_1 = 171$, $N_3 = .679$

(d) HELIUM; $N_1 = 68.3$, $N_3 = .735$

FIG.(5) TYPICAL SCHLIEREN PHOTOGRAPHS WITH VARIOUS MASS TRANSFER RATES.

predicted in reference 10. This result is in agreement with the generally accepted insensitivity of the pressure distribution to real gas effects for stagnation temperatures below roughly 5000°R.

2) The effect of large rates of injection is to lower the static pressure on the surface of the cone.

3) At a value of $\tilde{N}_R = 2.2 \times 10^4$, alteration of the pressure distribution on the cone surface is observed for $N_1 \geq 73.7$ for nitrogen and $N_1 \geq 24.9$ for helium.

4) Examination of schlieren photographs with increasing injection rate and decreasing Reynolds number, indicates that the shock stand-off distance is increased and that this alteration occurs before an observable change in pressure distribution occurs.

In order to extrapolate the heat transfer data presented here to different flow conditions, the combinations of injection rate and Reynolds number for which the pressure distribution is essentially unaltered must be estimated. Since the change in pressure distribution is associated with a radical change in the shock stand-off distance, a theoretical analysis leading to the prediction of the dependence of shock stand-off distance on mass transfer has been carried out and presented in Appendix I. This analysis predicts that the shock stand-off distance depends on an inviscid parameter $N_3 \equiv m_c(\theta_w W_e)^{\frac{1}{3}} / [R_o^2 (W_c p_{s_e} \rho_{s_e})^{\frac{1}{3}}]$ which can be formally identified as $N_3 \equiv N_1 (\theta_w W_e / \tilde{N}_R W_c)^{\frac{1}{3}}$. * Accordingly, there are presented in Figure 6 the variations with this parameter of Δ/R_o as obtained from the schlieren photographs. It will be observed that the correlation of the experimental data for both helium and nitrogen is good, and that Δ/R_o is increased by an order of magnitude by injection. Also presented in Figure 6 are the theoretical predictions of Δ/R_o given in Appendix I and based either on a consistent theory or on an empirical correction of the velocity gradient. It will be noted that both theoretical predictions agree well with the data although the empirical correction leads to somewhat better agreement.

Since the shock stand-off distance was found to be dependent on N_3, it was of interest to see if the shock shape and the pressure distribution on the cone can be correlated in terms of N_3. Comparison of Figures 5c and 5d and of other schlieren photographs wherein N_3 is roughly constant although N_1 and the coolant fluids are different, indicates that the correlation between shock shapes is good.

---

*Note that μ_{s_e} drops out of N_3 so that it is independent of viscosity and is thus an inviscid flow parameter.

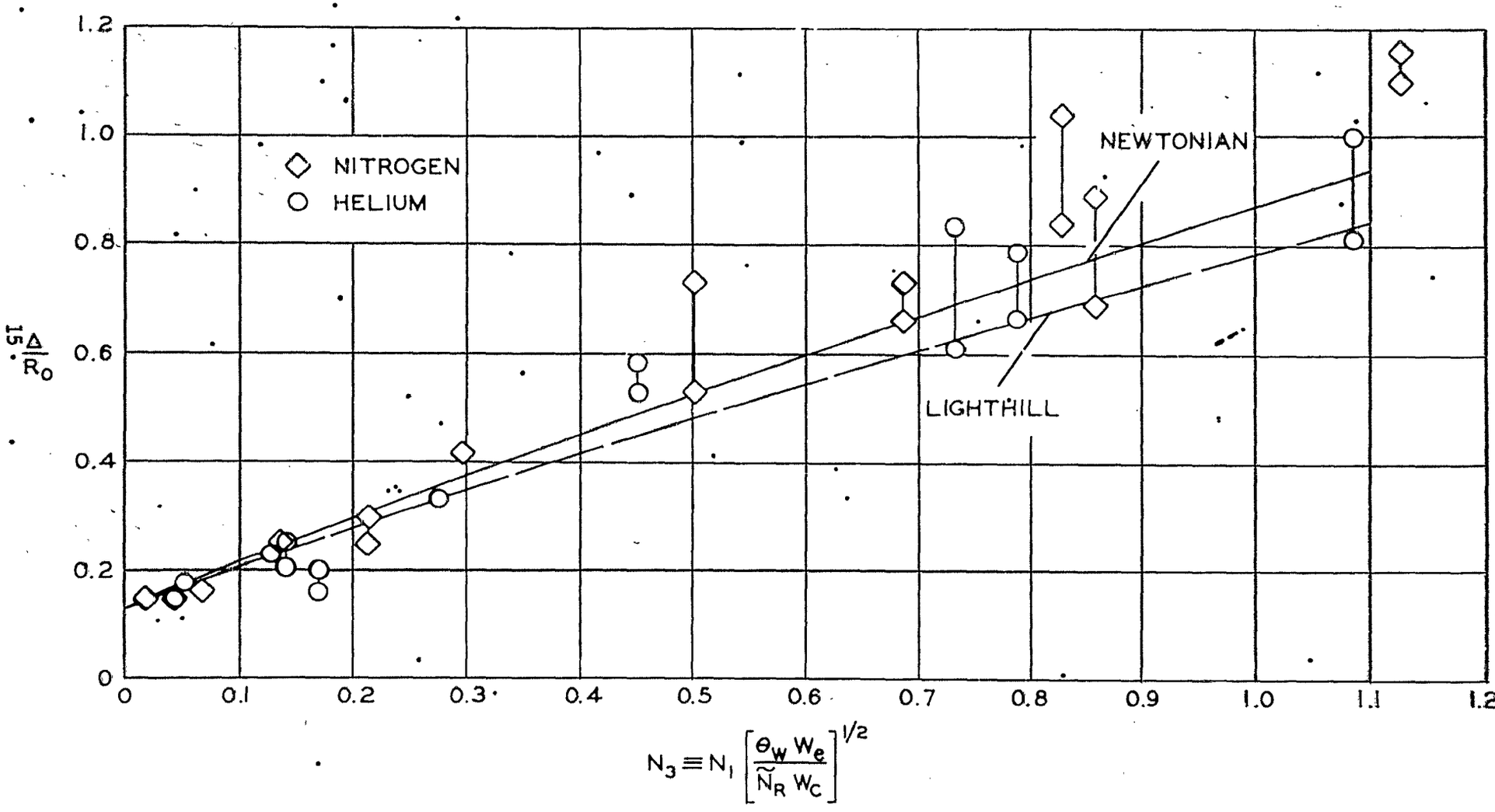

FIG.(6) VARIATION OF SHOCK STAND-OFF DISTANCE WITH INJECTION RATE

A careful study of the corresponding pressure distributions indicated that the experimental accuracy was not sufficient to establish N_3 as the correlation parameter for the pressure distribution. The correlation of shock shape with N_3 implies, however, that more accurate pressure measurements would confirm the correlation of pressure distribution in terms of N_3.

Now consider the value of N_3 which leads to an observable alteration of the pressure distribution. Because of experimental error it is difficult to select a precise value therefor; however, the aforementioned careful study of the pressure distributions leads to the result which is shown in Figure 7, and which defines roughly the critical values of N_3, namely, $1/4 \leq N_3 \leq 1/3$. Thus, for values of N_3 less than these, the pressure distribution is unaltered, the flow is of the boundary layer type, and the parameters N_1 and $\tilde{N}_R$ can be employed in determining the heat transfer for other than test conditions.

Heat Transfer

The heat transfer data for all tests are presented in Figures 8a-8m in terms of the heat transfer parameter N_2 versus N_1 at each thermocouple location. Data for each gas and the value of $\tilde{N}_R$ for each test are presented so that the Nusselt number at each measuring station and in each test can be explicitly determined if desired.

The interpretation of these heat transfer results is complicated by two effects: the alteration of the pressure distribution by injection as related to the parameter N_3 and the occurrence of transition. If neither of these two effects were present, it would be expected that N_2 would monotonically decrease with increasing N_1 at all thermocouple locations except those far downstream where N_2 would be expected to be independent of N_1.

In discussing these effects it is convenient to consider a fixed $\tilde{N}_R$ and a fixed thermocouple location. The observed reduction in static pressure on the cone might a priori be expected to lead to further reductions in heat transfer with increasing N_1. However, the response of the relatively thick, inner layer of injected gas to simultaneous viscous shear and to pressure gradient is complex; indeed, it will be seen that for the case of helium injection involving a different ratio of specific heats, the alteration of pressure distribution is accompanied by an increase in heat transfer. If transition is associated with increasing N_1, the heat transfer would be expected to increase. To assist in interpretation, the data in Figures 8a-8m

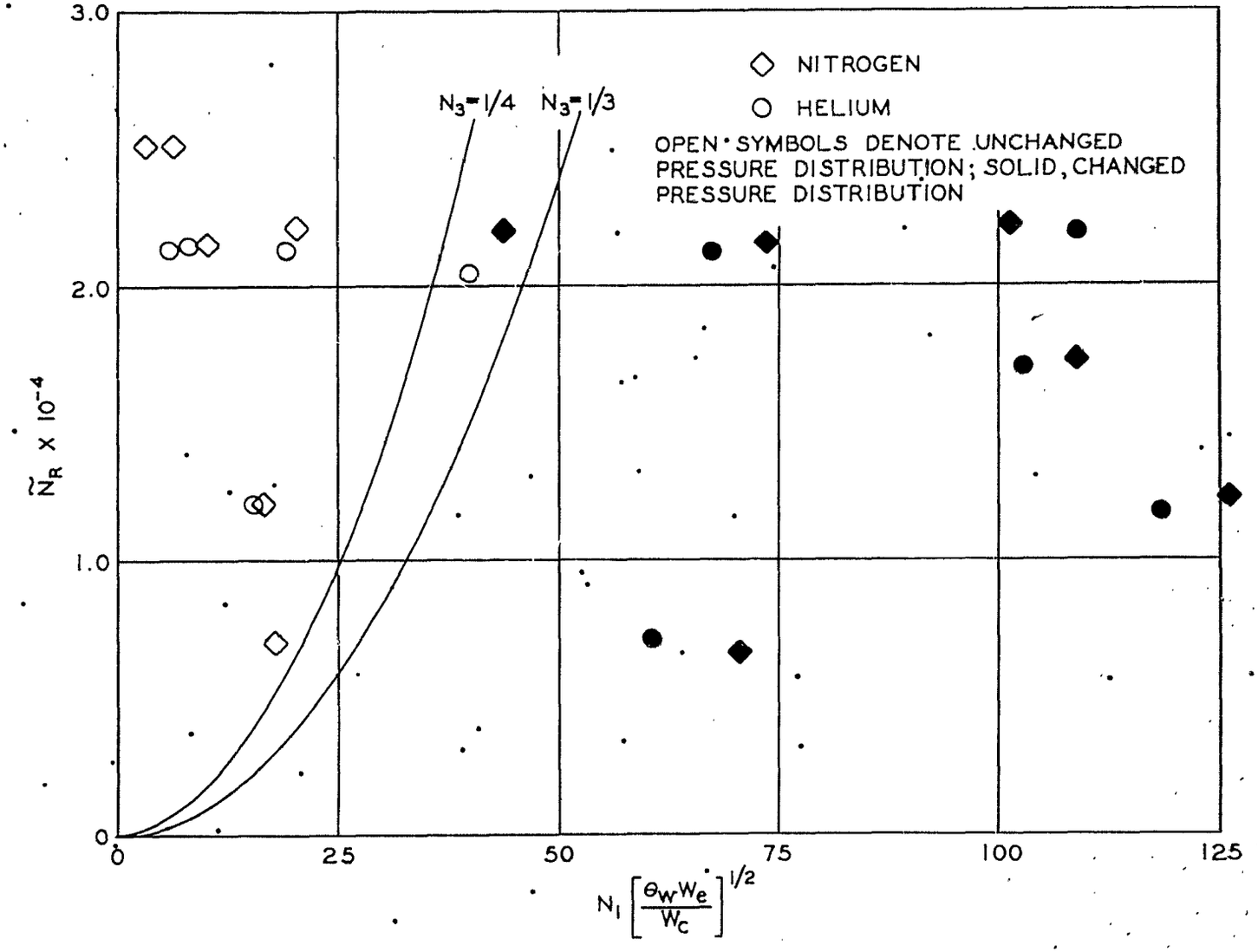

FIG. (7) CRITICAL REYNOLDS NUMBER VS MASS TRANSFER

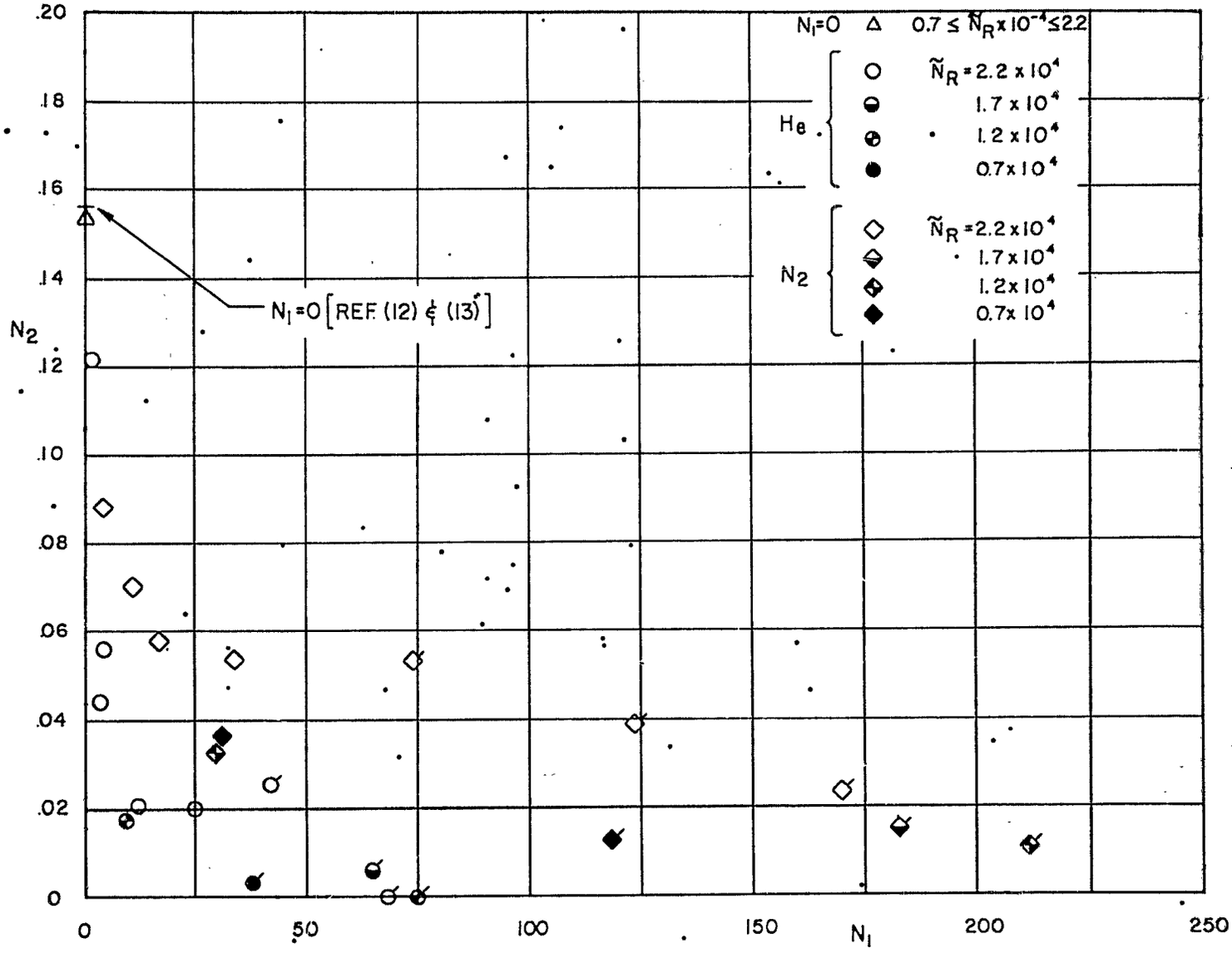

FIG. (8) VARIATION OF HEAT TRANSFER WITH MASS TRANSFER. (a) $\bar{x} = 1.85$

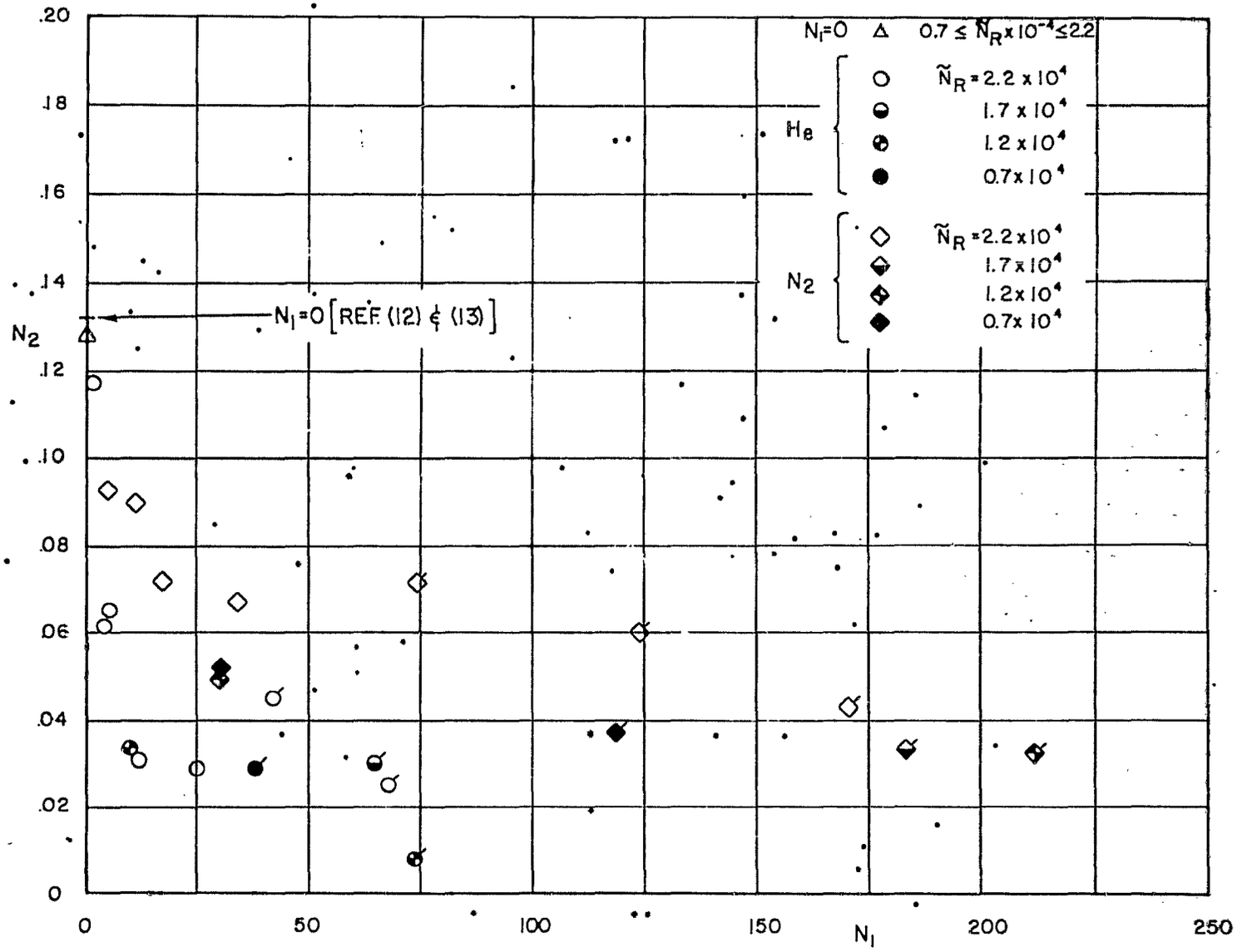

FIG. (8) VARIATION OF HEAT TRANSFER WITH MASS TRANSFER. (b). $\bar{x} = 2.84$

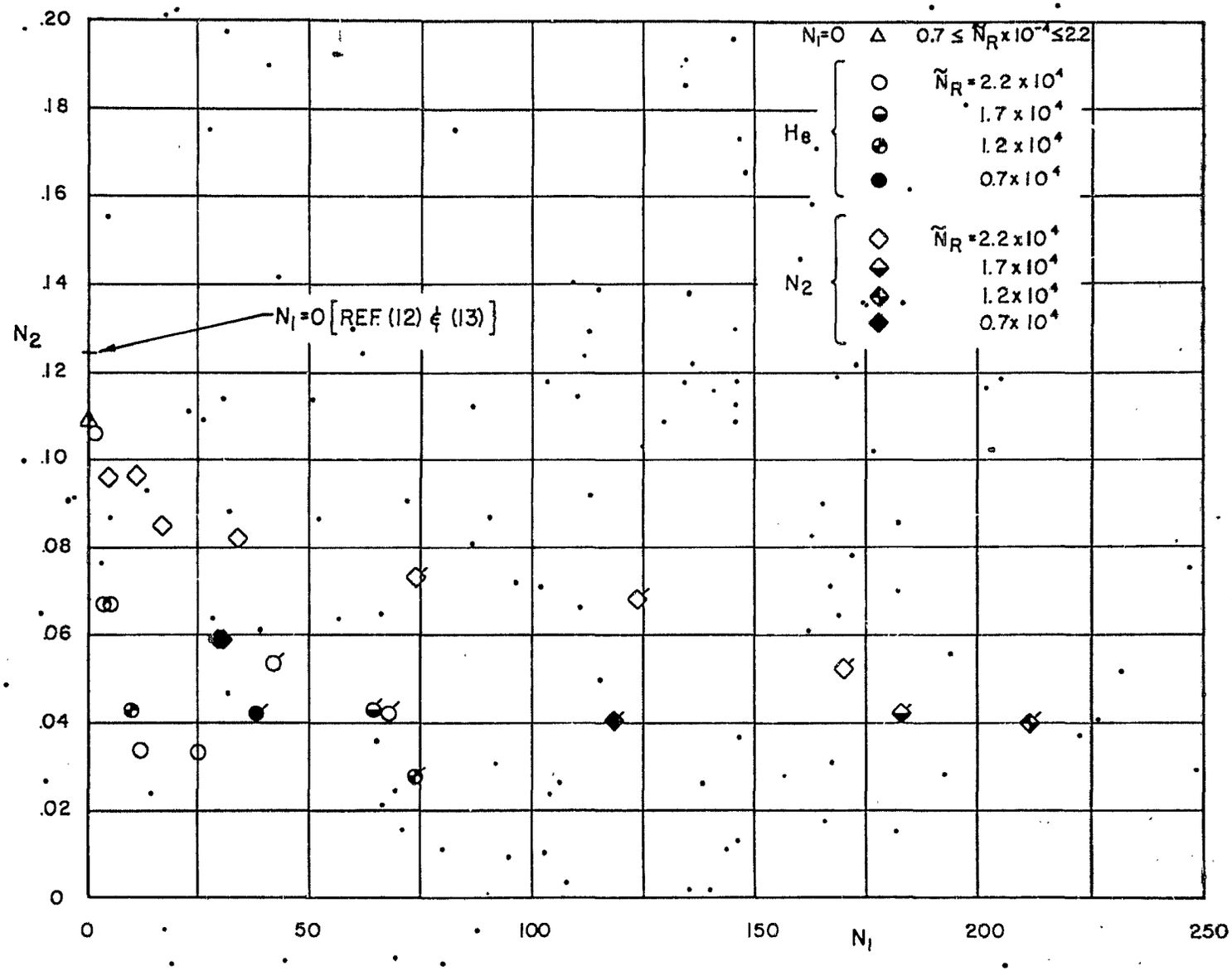

FIG. (8) VARIATION OF HEAT TRANSFER WITH MASS TRANSFER. (c) $\bar{x}=3.85$

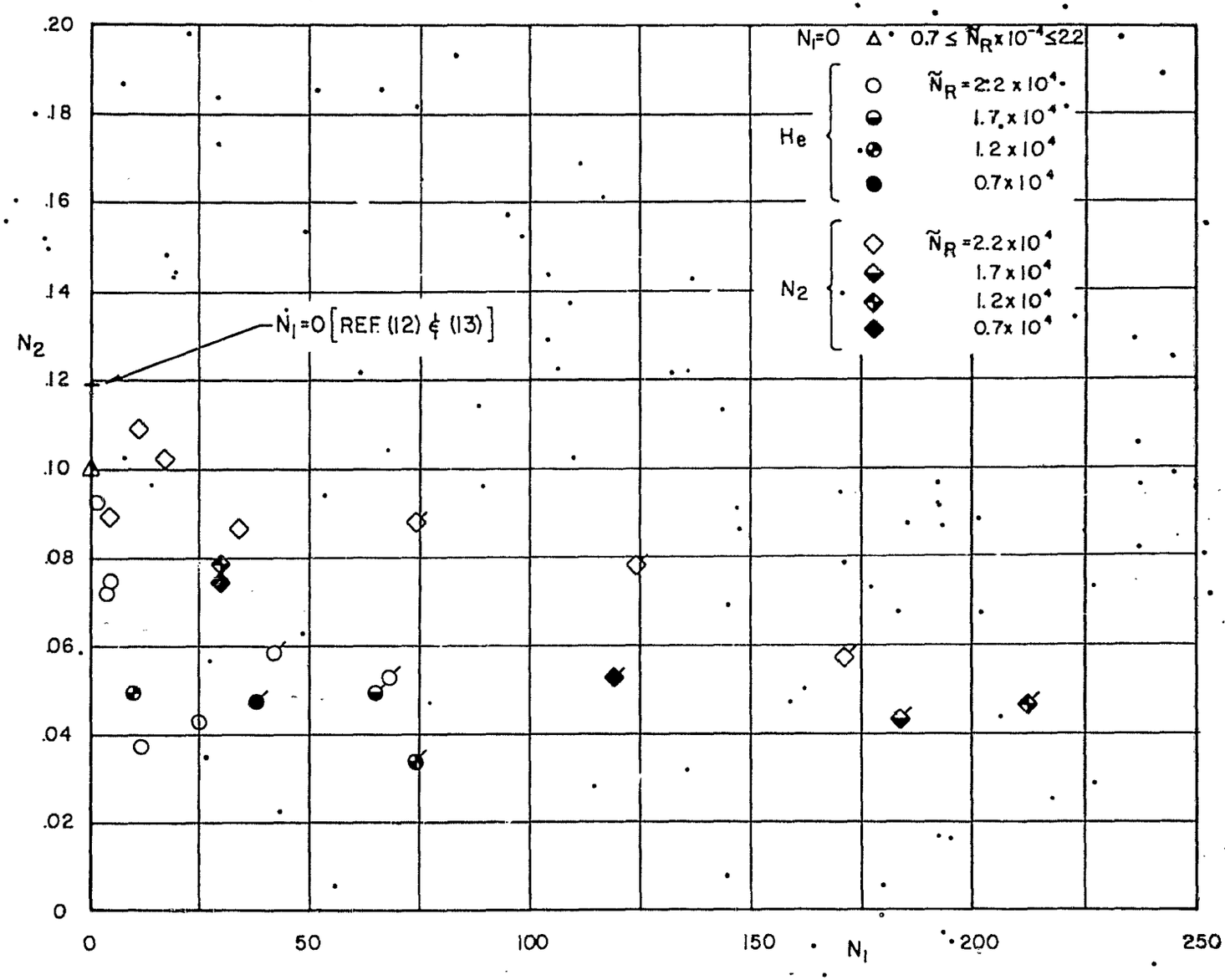

FIG. (8) VARIATION OF HEAT TRANSFER WITH MASS TRANSFER. (d) $\bar{x}$ = 4.84

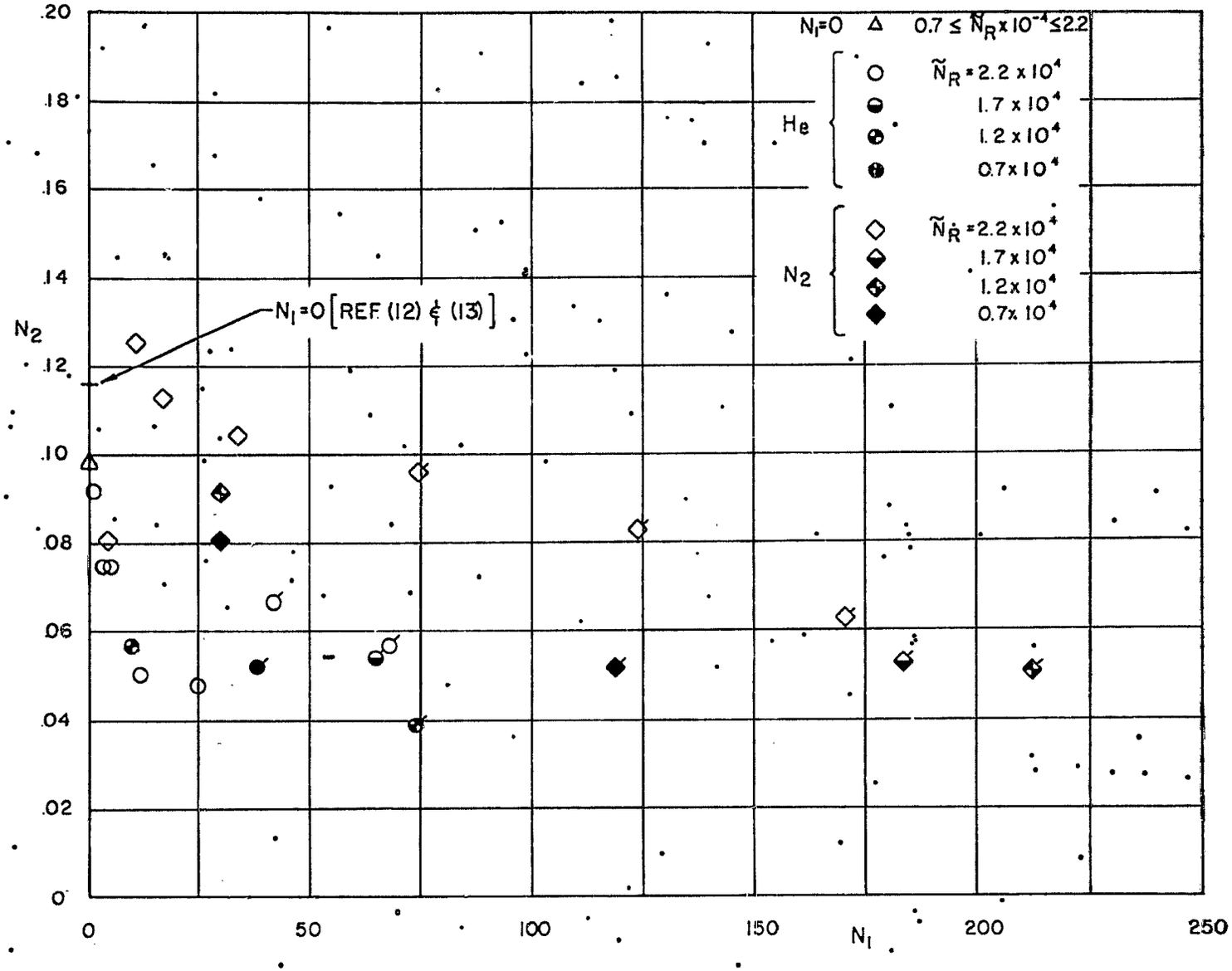

FIG. (8) VARIATION OF HEAT TRANSFER WITH MASS TRANSFER.(e) $\bar{x}=5.84$

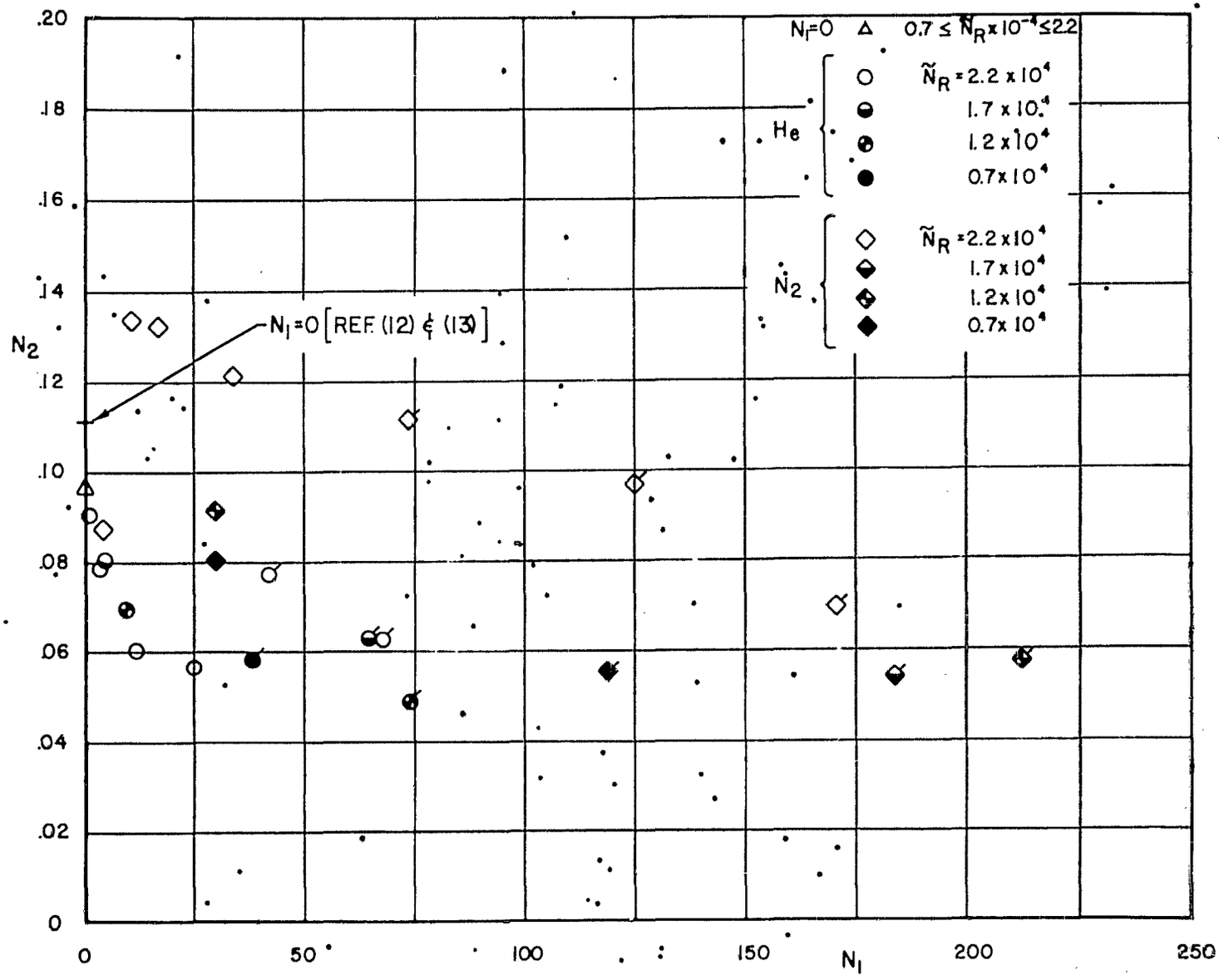

FIG. (8) VARIATION OF HEAT TRANSFER WITH MASS TRANSFER.(f) $\bar{x}$=6.85

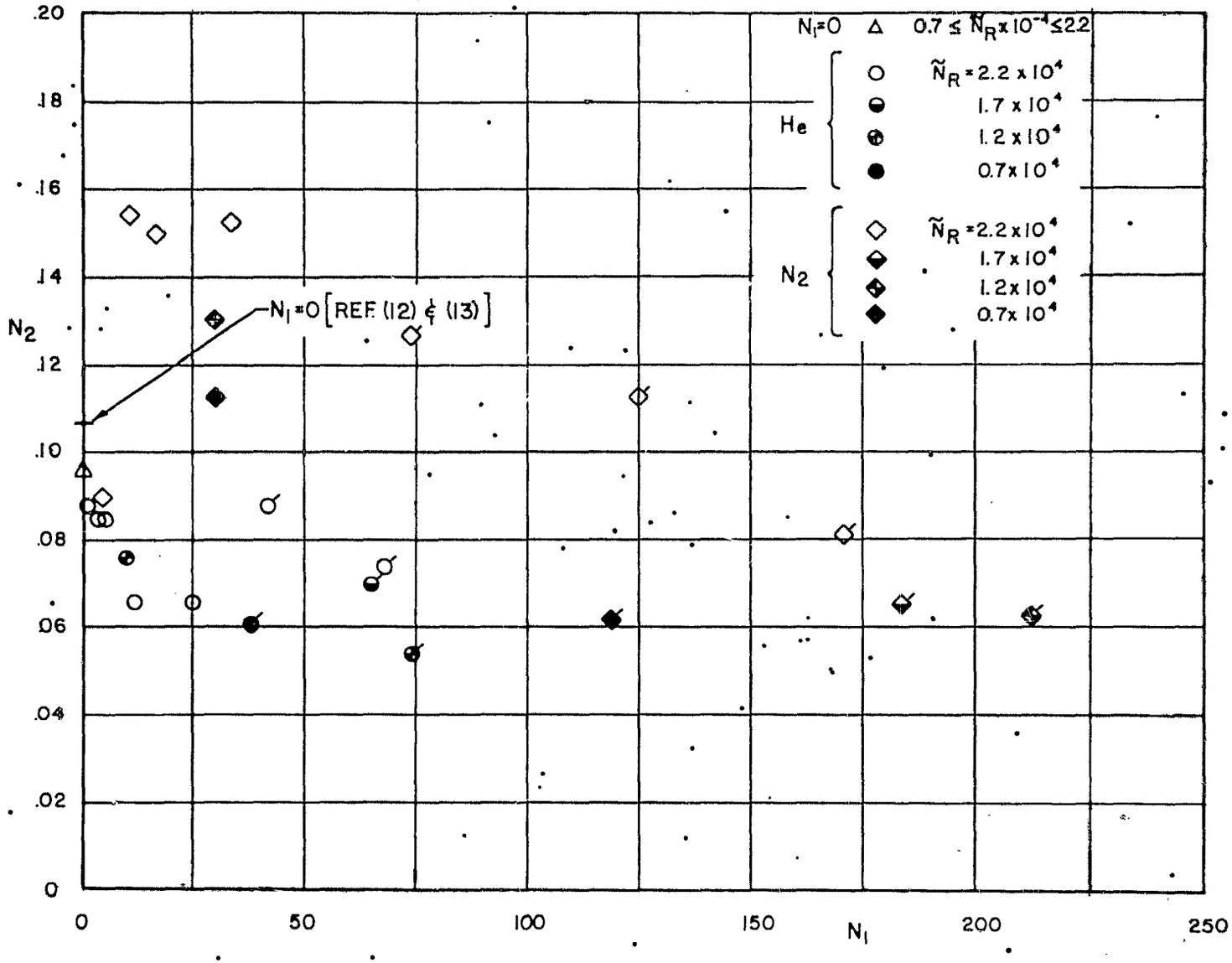

FIG. (8) VARIATION OF HEAT TRANSFER WITH MASS TRANSFER.(g) $\bar{x}$=7.84

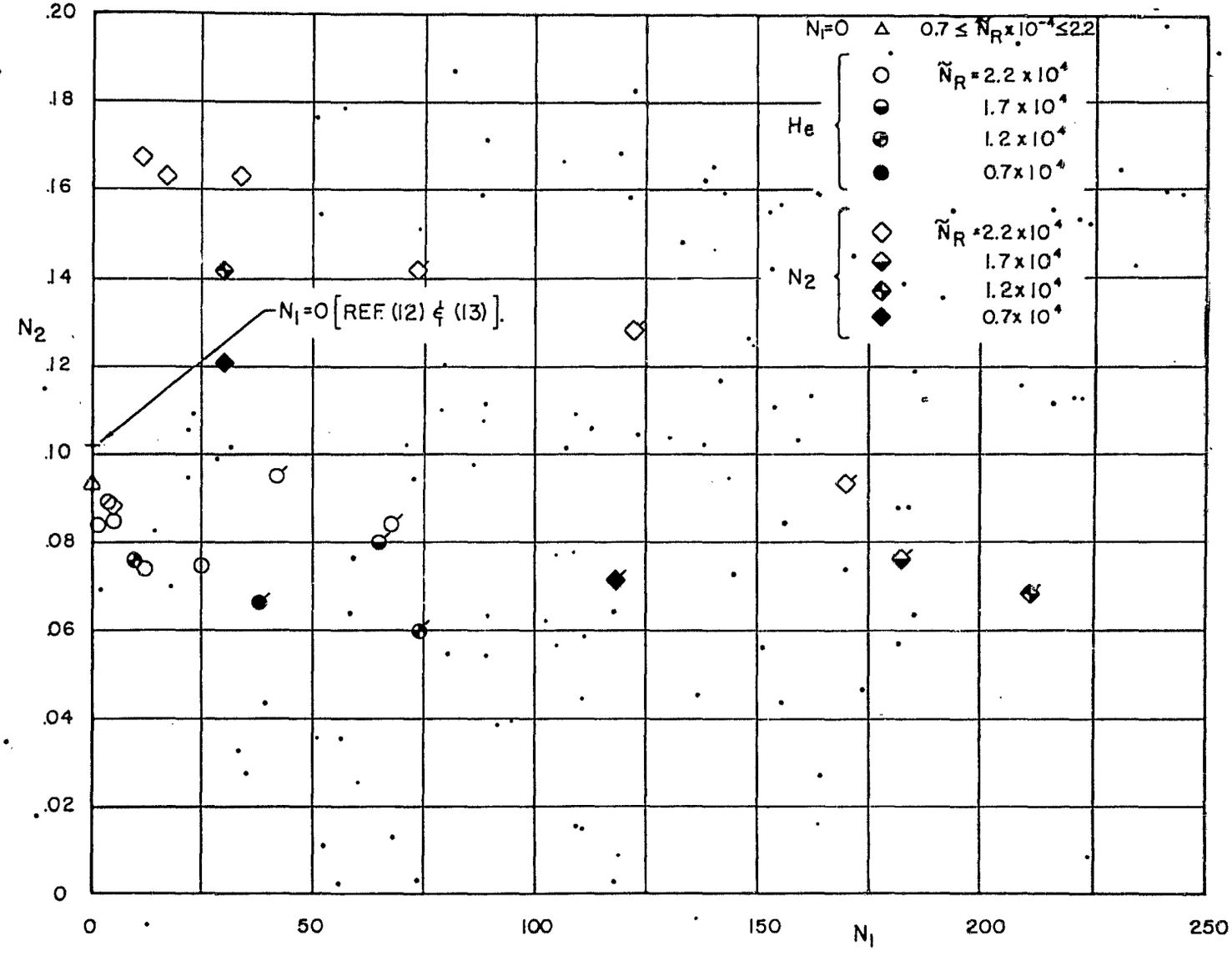

FIG. (8) VARIATION OF HEAT TRANSFER WITH MASS TRANSFER. $(h)\bar{x}=8.85$

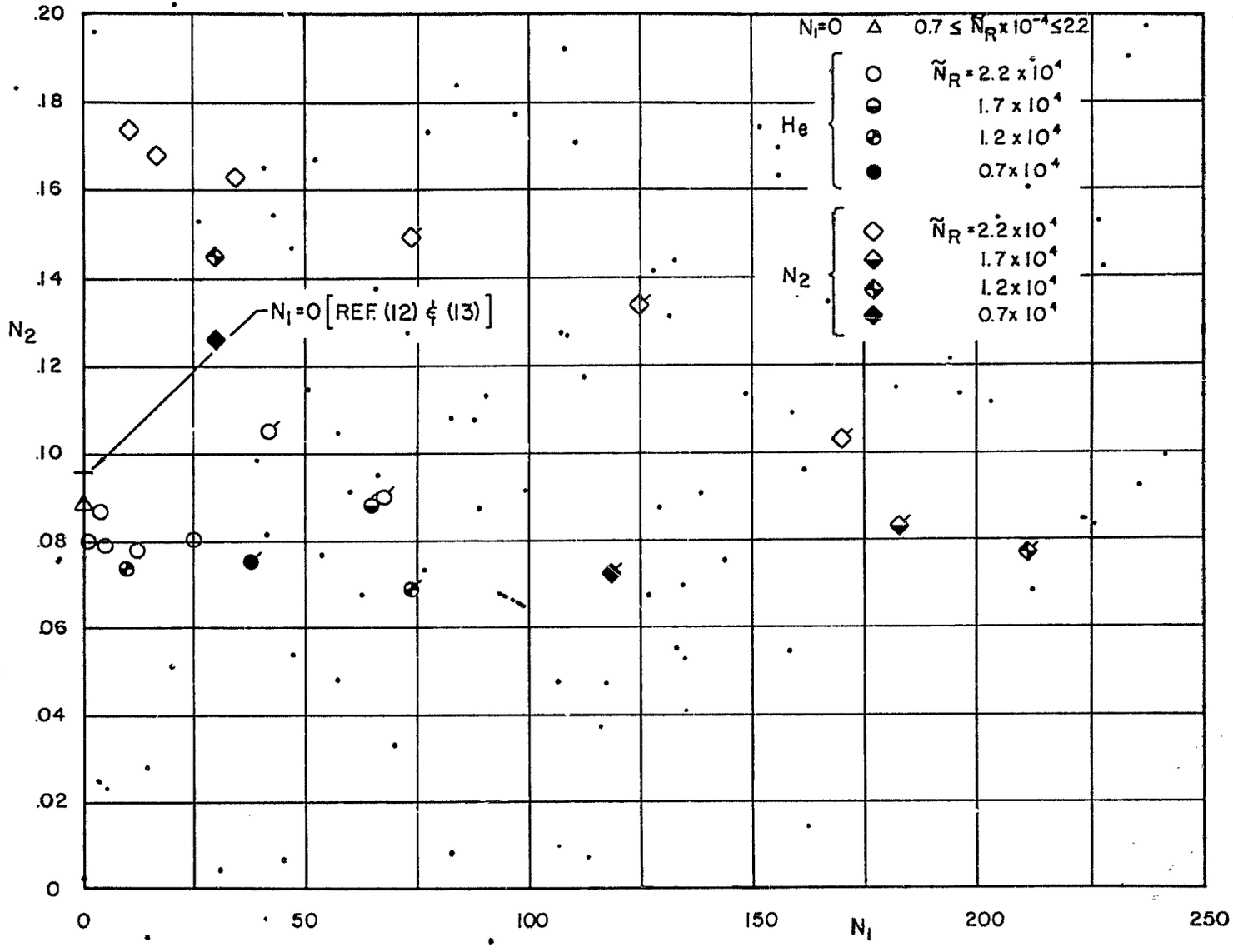

FIG. (8) VARIATION OF HEAT TRANSFER WITH MASS TRANSFER.(i) $\bar{x}=9.84$

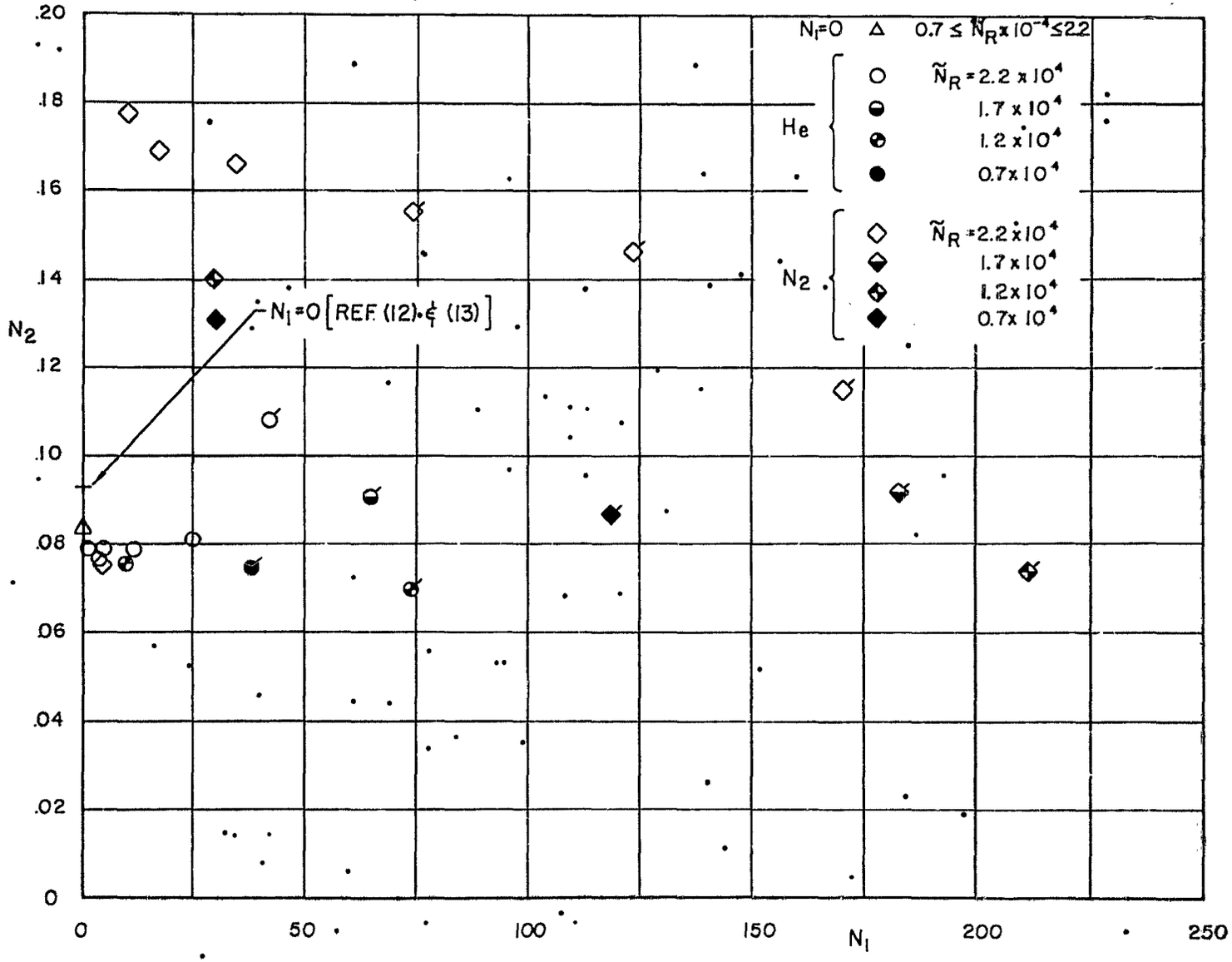

FIG. (8) VARIATION OF HEAT TRANSFER WITH MASS TRANSFER. $(j)\bar{x}=10.84$

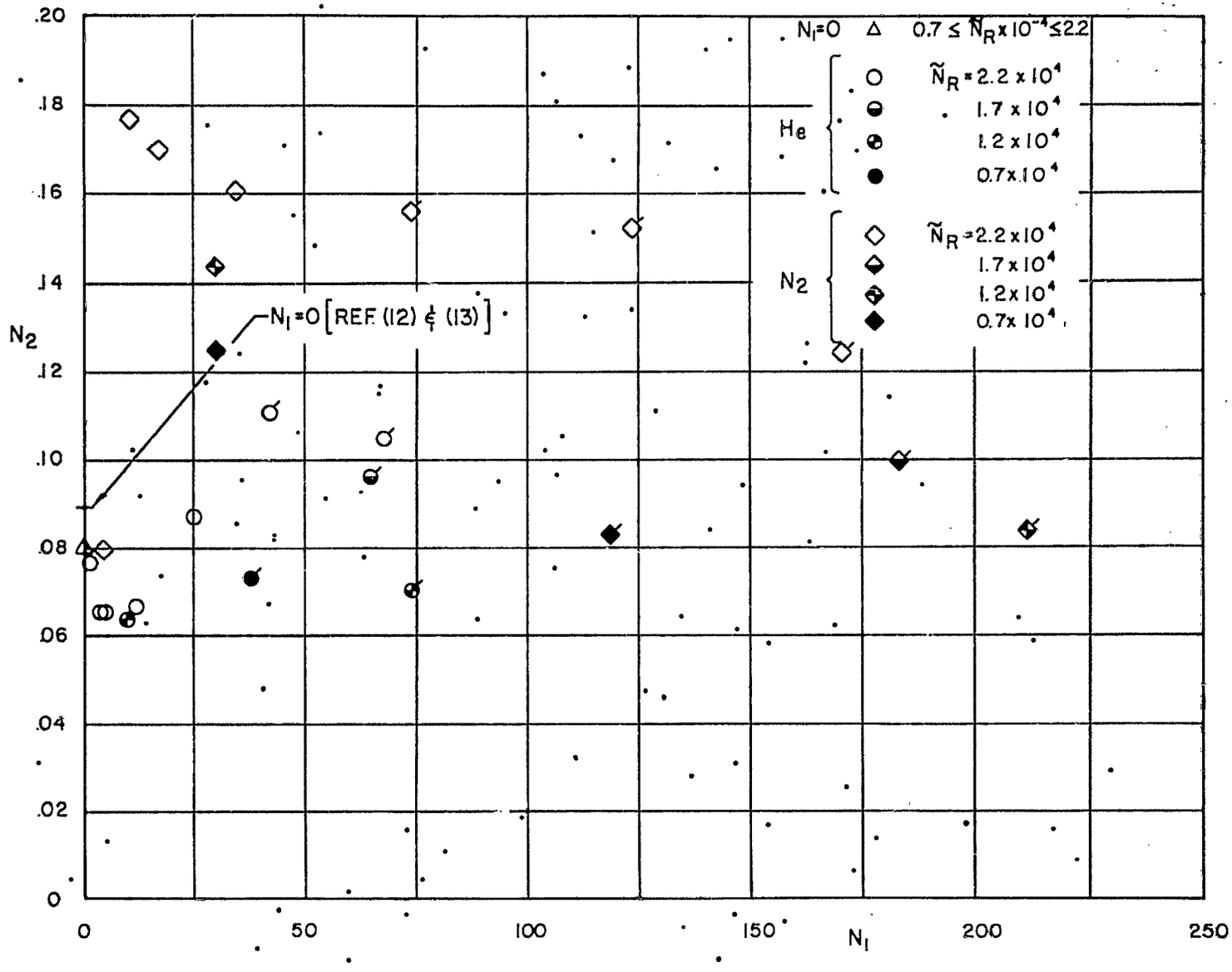

FIG. (8) VARIATION OF HEAT TRANSFER WITH MASS TRANSFER. (k) $\bar{x} = 11.84$

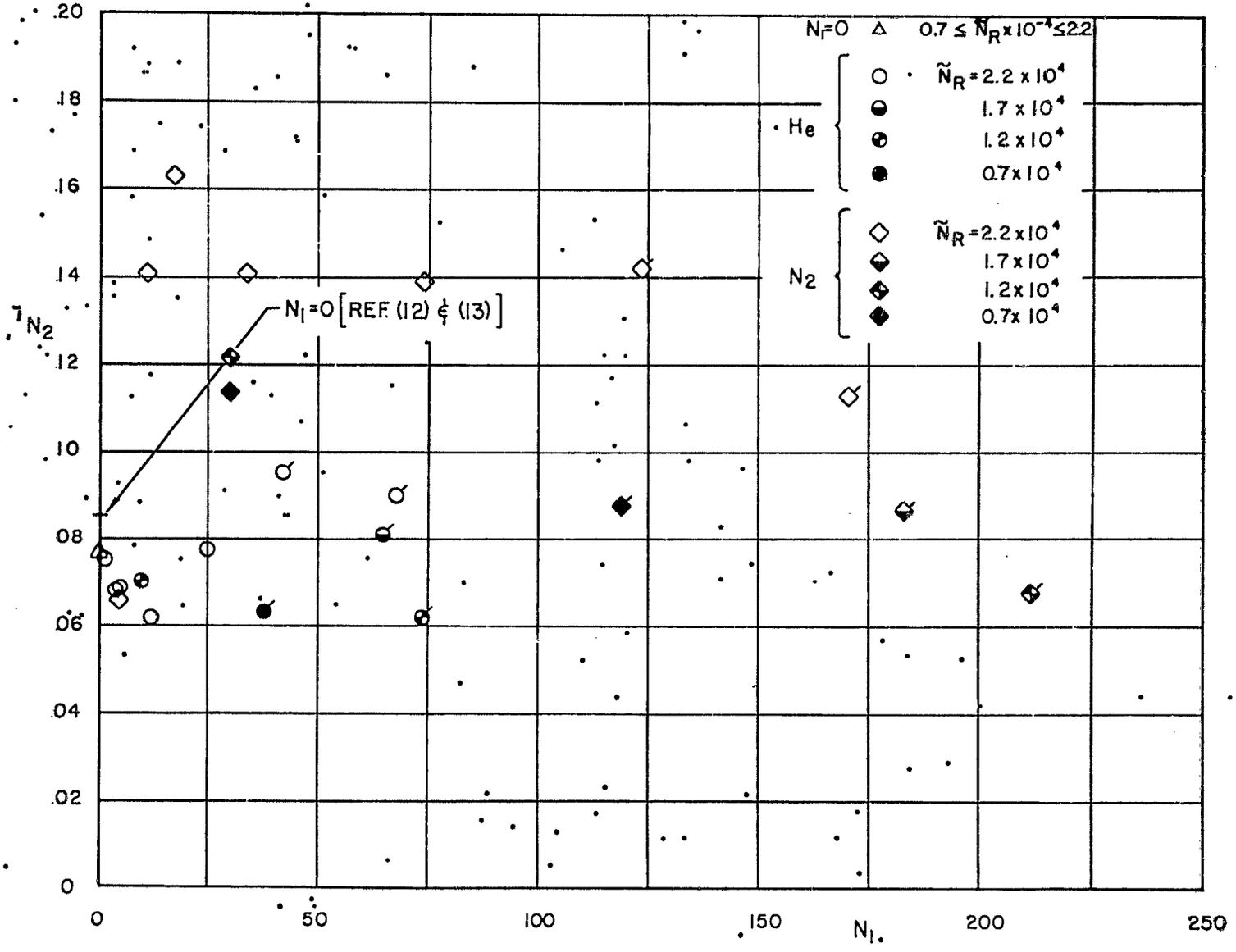

FIG. (8) VARIATION OF HEAT TRANSFER WITH MASS TRANSFER. (1) $\bar{x}$ =12.84

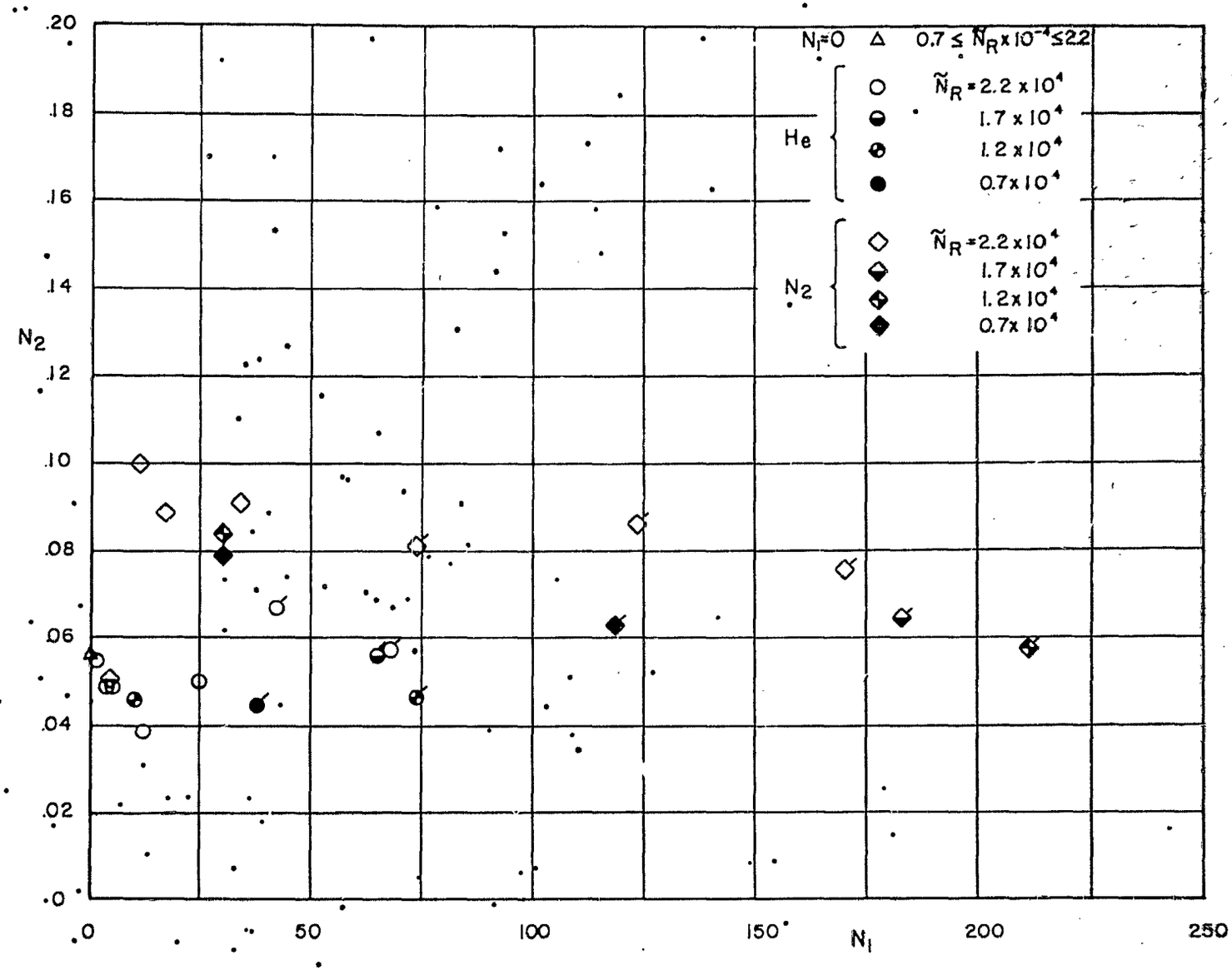

FIG. (8) VARIATION OF HEAT TRANSFER WITH MASS TRANSFER. (m) $\bar{x}$ = 13.25

have been identified with a flag if $N_s \geq 1/3$, i.e., the value of N_s resulting in an observable change in pressure distribution.

Consideration of Figures 8a-8m indicates the following:

1) For a given N_1 the reduction in N_2 is considerably greater for helium than for nitrogen.

2) For helium, N_2 decreases sharply with increasing N_1 for $N_1 < 25$ and for $\bar{s} < 8.85$. For $N_1 > 25$ and $\bar{s} > 8.85$, N_2 is relatively insensitive to N_1. For a fixed $\tilde{N}_R$ and increasing $\tilde{N}_1$, the heat transfer increases when $N_3 \geq 1/3$; further increases in N_1 lead to a second decline in heat transfer. From a consideration of the data for fixed N_1 but varying $\tilde{N}_R$, it is not possible to determine if transition is occurring in these tests.

3) For nitrogen there appears to be no increase in heat transfer associated with the alteration in pressure distribution, i.e., with $N_3 \geq 1/3$. However, the difference in the values of N_2 for a given N_1 but different $\tilde{N}_R$ implies that transition is present.* Indeed, there appears to be only one nitrogen test in which both laminar flow and unaltered pressure distribution occurred. Transition is seen to lead to heat transfer rates which are higher with mass transfer than without.

4) With values of $N_1 \tilde{=} 5$ for helium the heat transfer over the entire cone corresponds to $N_2 \tilde{=} 0.08$ or less. This should be compared to $N_2 = 0.84$ which exists at a stagnation point without mass transfer (cf. references 1, 2 and 9). Note that on the porous regions the heat transfer is zero for relatively small values of N_1 as may be inferred from reference 2. Thus as a heat protection system the configuration studied here is quite effective.**

It is of interest to consider two cross-plots of the data of Figures 8a-8m. In Figure 9 there are given the distributions of N_2 with $\bar{x}$ for those tests in which the inviscid flow was considered unaltered by injection ($N_3 \leq 1/3$) and in which laminar flow prevailed. Also shown thereon is the theoretically predicted distribution of N_2 for zero injection obtained from a combination of the analyses of references 12 and 13. The distribution of heat transfer relative to the stagnation point value is computed from reference 12 with a constant isentropic exponent of 1.32 and the

---

* The transition data will be discussed in detail below.

** It may be of interest to note that if $R_o = 0.5$ ft., h=50,000 ft. and $V_\infty \tilde{=} 8000$ fps, $m_c = 0.19$ lbs/sec for $N_1 = 5.0$.

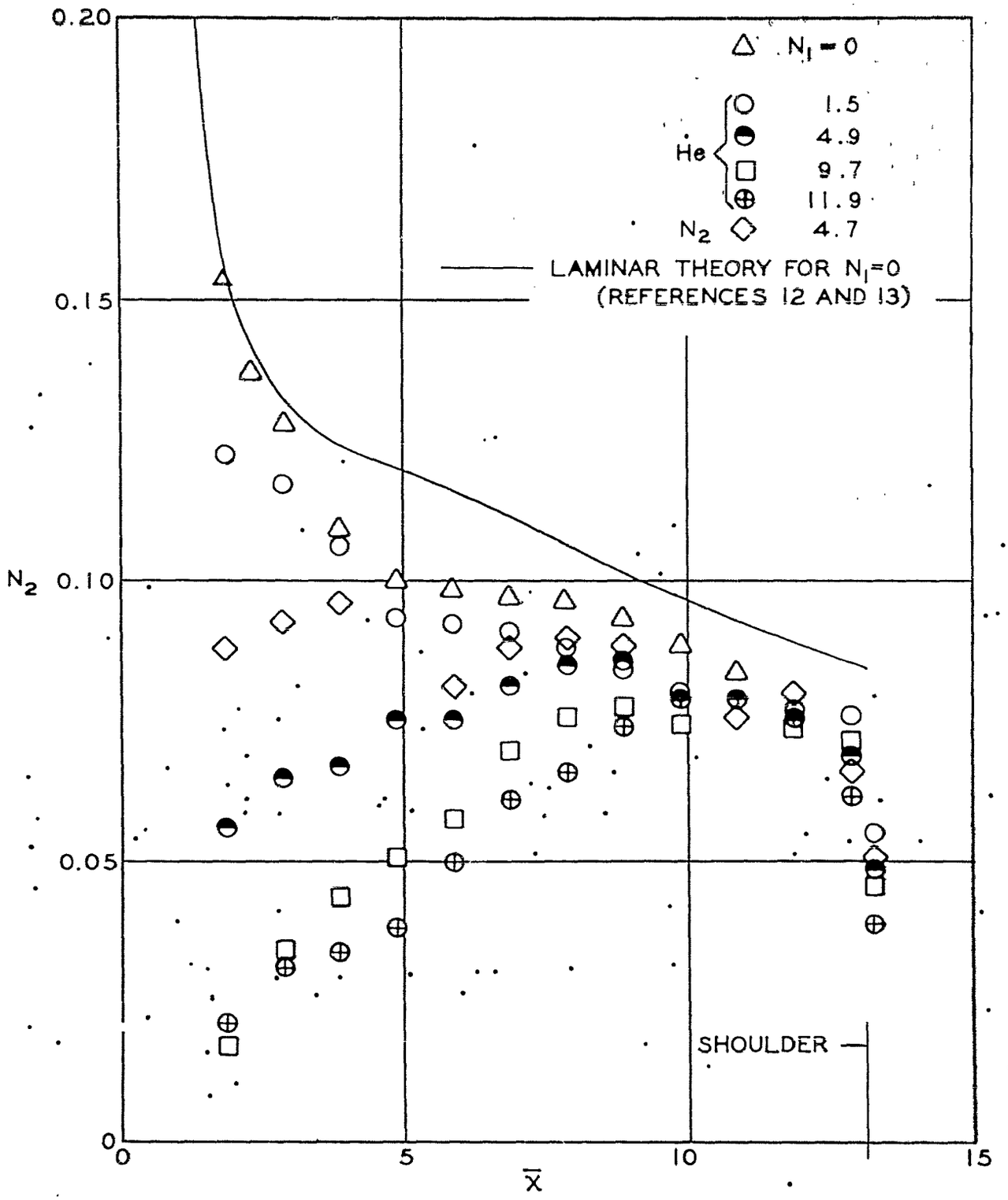

FIG.(9) DISTRIBUTION OF HEAT TRANSFER FOR $N_3 < 1/4$

measured pressure distribution; the stagnation point value is obtained from reference 13. The stagnation pressure behind a normal shock was assumed to prevail over the entire body. It will be noted that the agreement between theory and experiment for zero injection is within 20%. It will also be seen from Figure 9 that substantial reductions in laminar heat transfer over extended portions of the cone occur with helium injection. The influence of injection of helium is seen to persist to some extent even around the junction of the cone-cylinder.

A second cross-plot of interest is shown in Figure 10; there the distributions of Nusselt number N_{Nu} with $\bar{x}$ are given for nitrogen as a coolant and for a fixed Reynolds number, $\tilde{N}_R = 2.2(10^4)$. In addition to the experimental data, there are shown the theoretical predictions for laminar flow as discussed above in connection with Figure 9 and for fully developed turbulent flow. The flat plate-reference-enthalpy (F. P. R. E.) method (cf. reference 14) was employed for turbulent flow with normal shock stagnation pressure and with two pressure distributions, corresponding to $N_3 \lesssim 1/4$ and for $N_3 = 1.13$. The same method was also employed for the pressure distribution corresponding to $N_3 \lesssim 1/3$ but with oblique shock stagnation pressure.

Consideration of Figure 10 indicates that most of the data obtained with nitrogen involve transitional and turbulent flow. The heating rates over the front portion of the cone are reduced by the mass transfer but for $\bar{x} \gtrsim 5$ the effect of mass transfer is to cause earlier transition and therefore heating rates which are greater with than without mass transfer. The maximum heating rates obtained experimentally are greater than those predicted by the F. P. R. E. method when the stagnation pressure of the flow external to the boundary layer corresponds to that behind a normal shock. However, if the stagnation pressure is assumed to be that behind the oblique shock, the predicted turbulent heating without mass transfer is greater than determined experimentally. The results in reference 15 for the interaction of a turbulent boundary layer with the vortical layer induced by the bow shock indicate that some influence may be expected for $\bar{x} \gtrsim 10$ under the test conditions of Figure 10 with no mass transfer. Therefore, the observed rates with mass transfer may involve vortical interaction. In view of this complication, it is not possible to ascertain the influence of the mass transfer on the heat transfer after transition has occurred.

Transition Behavior

From a representation of the heat transfer data for nitrogen in the form shown in Figure 10 it is possible to estimate the location of transition for various rates of injection and various Reynolds numbers. The results are shown in Figure 11 for the test data corresponding to $N_3 \lesssim 1/3$; as seen qualitatively from Figure 10 and discussed previously, injection results in transition at a smaller value of $\bar{x}$. It can

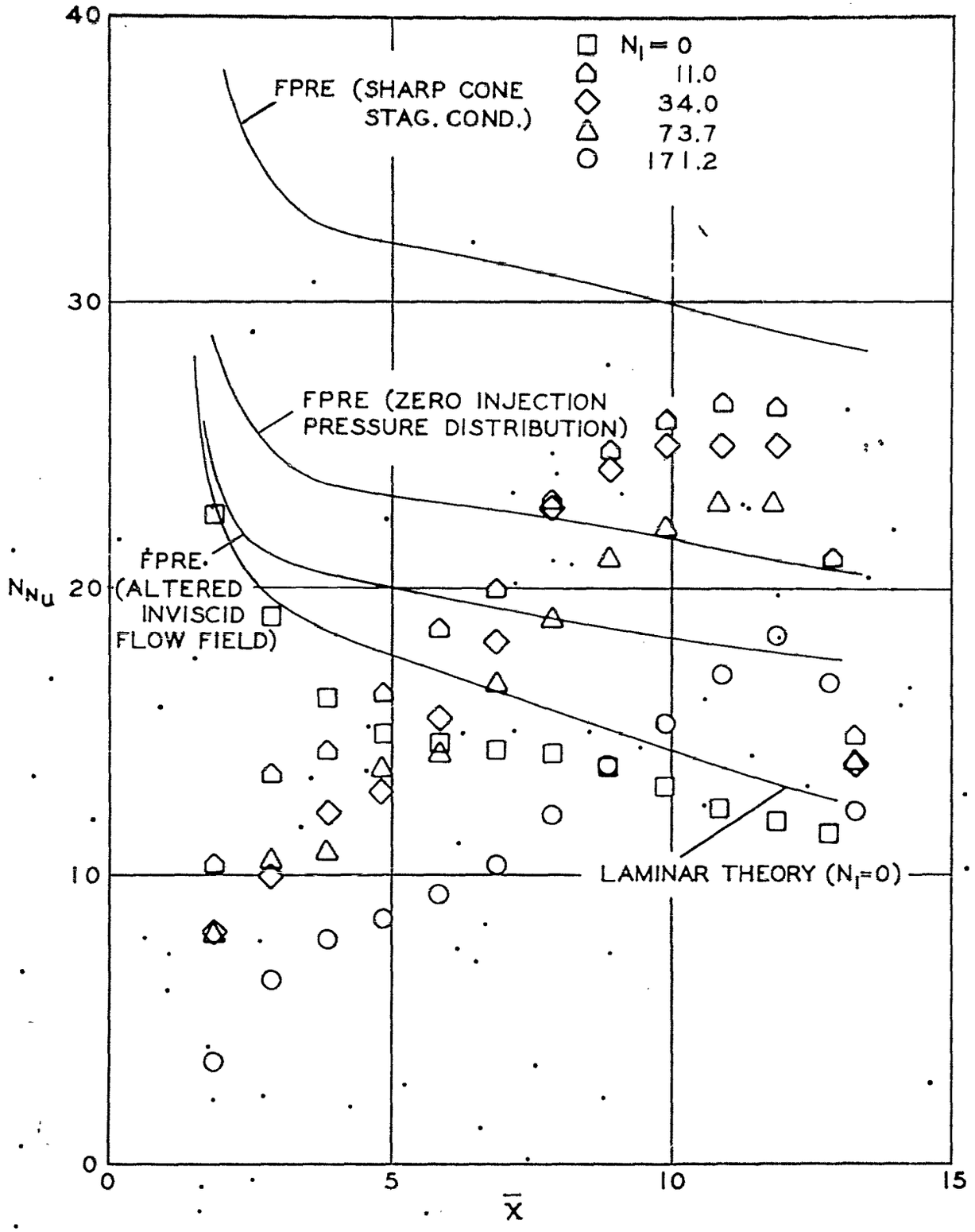

FIG. (10) SURFACE DISTRIBUTION OF NUSSELT NUMBER FOR $\tilde{N}_R \simeq 2.2 \times 10^4$ (NITROGEN)

also be seen from Figure 11 that transition moves downstream ($\tilde{x}$ increasing) as the Reynolds number decreases.

It is customary to consider transition behavior in terms of a Reynolds number based on momentum thickness (cf. for example reference 14). However, the analysis of the data of Figure 11 in these terms awaits a theoretical treatment of the downstream behavior of the laminar boundary layer. Presently, the data of Figure 11 must be considered only indicative.

IV. CONCLUSIONS

There has been carried out an investigation of the influence of localized mass transfer at the nose of a slender cone. Two gaseous coolants were considered, nitrogen and helium. The experimental research involved tests in the Mach number 8.0 wind tunnel at PIBAL. The rate of coolant mass flow and the Reynolds number of the main stream were varied widely. Measurements were made of the pressure and heat transfer distributions; schlieren photographs were taken.

Three effects of the mass transfer are examined: the alteration of shock shape and pressure distribution, of heat transfer to the downstream conical surface, and of transition. With respect to the first effect a theoretical analysis of the influence of mass transfer on the shock stand-off distance has been carried out. The model for the shock layer proposed by Lighthill is combined with a model suggested by the results of reference 2 for the viscous layer formed by the coolant. Accordingly, the flow at the nose is characterized by two incompressible rotational layers with a discontinuity in tangential velocity at the interface. This analysis which is applicable to both nitrogen and helium suggests an inviscid flow parameter N_3 which is related to the mass transfer and which is shown to correlate the observed alteration in shock stand-off distance by coolant injection.

The mass transfer is found to have a negligible effect on the pressure distribution on the cone for combinations of mass transfer and Reynolds numbers resulting in $N_3 \leq 1/3$. Thus for flows satisfying this inequality laminar boundary layer effects are correlated by the parameters presented in reference 1, i.e., N_1 and $\tilde{N}_R$. For flows corresponding to $N_3 > 1/3$ the pressure distribution is altered by the mass transfer so that no extrapolation of results to flow conditions other than those of the tests is possible.

With respect to the influence of mass transfer on heat transfer it is found as shown previously that helium is the superior coolant. With helium at relatively low rates of coolant flow the peak heating occurs downstream on the cone and is an order of magnitude less than would occur at the stagnation point if there were no mass transfer.

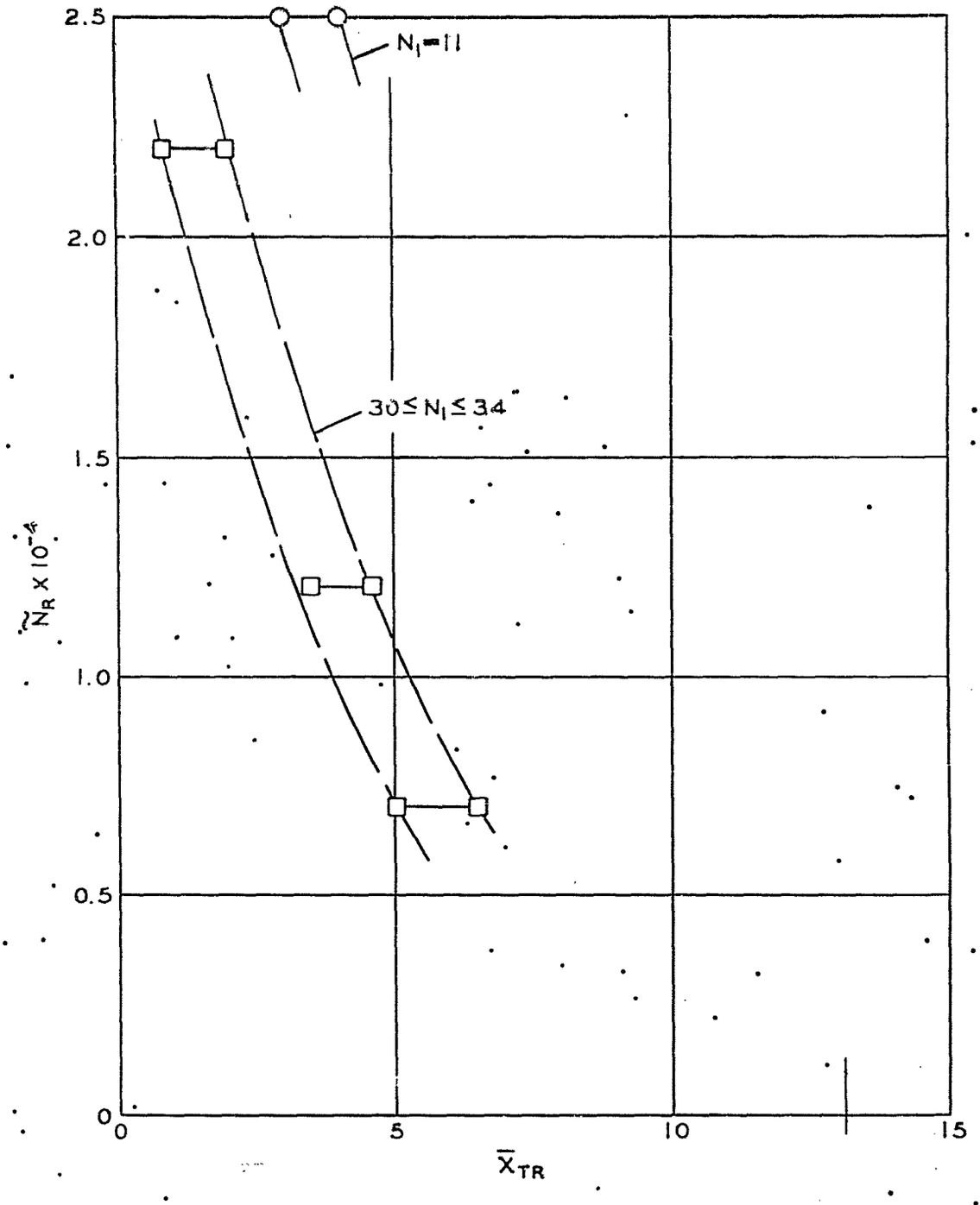

FIG.(11) VARIATION OF TRANSITION POINT WITH INJECTION RATE AND REYNOLDS NUMBER (NITROGEN INJECTION)

The injection of nitrogen is found to lead to earlier transition. Thus on the cone the peak heating with injection is greater than without injection although considerably less than at the stagnation point. The behavior of transition with injection is deduced from the heat transfer results; as might be expected transition moves forward on the cone with increasing mass transfer and increasing Reynolds number.

V. REFERENCES

1. Libby, P.A. and Cresci, R.J.: Experimental Investigation of the Downstream Influence of Stagnation Point Mass Transfer. Journal of the Aerospace Sciences, Vol. 28, No. 1, pp. 51-64, January 1961.

2. Libby, P.A.: The Homogeneous Boundary Layer at an Axisymmetric Stagnation Point with Large Rates of Injection. Polytechnic Institute of Brooklyn, PIBAL Report No. 605, WADD TR-435, August 1960. (Accepted for publication in the Journal of the Aerospace Sciences).

3. Libby, P.A. and Pallone, A.: A Method for Analyzing the Insulating Properties of the Laminar Compressible Boundary Layer. Journal of the Aeronautical Sciences, Vol. 21, No. 12, pp. 825-834, December 1954.

4. Rubesin, M.W. and Inouye, M.: A Theoretical Study of the Effect of Upstream Transpiration-Cooling on the Heat-Transfer and Skin-Friction Characteristics of a Compressible, Laminar Boundary Layer. NACA TN 3969, May 1957.

5. Howe, J.: Some Finite Difference Solutions of the Laminar Compressible Boundary Layer Showing the Effects of Transpiration Cooling. NASA Memo 2-26-59A, February 1959.

6. Pallone, A.: Non-Similar Solutions of the Compressible Laminar Boundary Layer Equations with Applications to the Upstream Transpiration Cooling Problem. AVCO Research and Advanced Development Division, RAD-TR-9-60-8, May 1960. (To appear in the Journal of the Aerospace Sciences).

7. Ferri, A. and Libby, P.A.: The Hypersonic Facility of the Polytechnic Institute of Brooklyn and Its Application to Problems of Hypersonic Flight. Polytechnic Institute of Brooklyn PIBAL Report No. 392, WADC TN 57-369, AD 130 809, August 1957.

8. Zakkay, V.: Status Report of the Hypersonic Facility of the Polytechnic Institute of Brooklyn. Polytechnic Institute of Brooklyn, PIBAL Report No. 602 (Presented at the Thirteenth Semi-Annual Meeting of the Supersonic Tunnel Association, Dallas, Texas, April 26-28 1960).

9. Zakkay, V.: Pressure and Laminar Heat Transfer Results in Three-Dimensional Hypersonic Flow. Polytechnic Institute of Brooklyn, PIBAL Report No. 447, WADC TN 58-182, AD 155 679, September 1958.

10. Vaglio-Laurin, R. and Trella, M.: A Study of Flow Fields About Some Typical Blunt Nosed Slender Bodies. Polytechnic Institute of Brooklyn PIBAL Report No. 623, December 1960.

11. Anonymous: Equations, Tables and Charts for Compressible Flow. NACA Report 1135, 1953.

12. Lees, L.: Laminar Heat Transfer Over Blunt-Nosed Bodies at Hypersonic Flow Speeds. Jet Propulsion, Vol. 26, No. 4, April 1956.

13. Fay, J.A. and Riddell, F.R.: Theory of Stagnation Point Heat Transfer in Dissociated Air. Journal of the Aerospace Sciences, Vol. 25, No. 2, pp. 73-85, February 1958.

14. Cresci, R.J.; MacKenzie, D.A. and Libby, P.A.: An Investigation of Laminar Transitional and Turbulent Heat Transfer on Blunt Nosed Bodies in Hypersonic Flow. Journal of the Aerospace Sciences, Vol. 27, No. 6, June 1960.

15. Ferri, A.: Some Heat Transfer Problems in Hypersonic Flow. Durand Centennial Conference on Aeronautics and Astronautics, Pergamon Press, 1960.

16. Lighthill, M.J.: Dynamics of a Dissociating Gas. Journal of Fluid Mechanics, Vol. 2, 1957.

17. Whitham, G.B.: A Note of the Stand-Off Distance of the Shock in High Speed Flow Past a Circular Cylinder. Communications on Pure and Applied Mathematics, Vol. X, 1957.

APPENDIX I - THE SHOCK STAND-OFF DISTANCE WITH STAGNATION POINT MASS TRANSFER

The shock stand-off distance has been determined for flow about a sphere by Lighthill (reference 16) and about a circular cylinder by Whitham (reference 17). Both analyses utilize the same approximations. These consist of:

(1) applying strong shock conditions which are valid for large free-stream Mach number;

(2) considering the flow field between the body and the shock to be incompressible and rotational; and

(3) assuming the shock to be a sphere or a circular cylinder.

It is generally accepted that these solutions accurately predict the shock stand-off distance but not the pressure distribution.

The purpose of the present analysis is to extend the results of Lighthill to include the effect of mass transfer from a spherical body. Note that the injection region is assumed to extend around the entire forward portion of the body. The treatment of a circular cylinder as presented by Whitham can also be extended to include mass transfer effects.

The flow is shown schematically in Figure 12. A spherical shock of radius $r_s = \Delta + R_o$ is associated with a sphere of radius R_o. The flow between the shock and the body is divided into two regions by an interface of radius r_o. In the outer layer between the shock and the interface the flow is of constant density and is rotational because of the shock curvature. The inner layer is between the interface and the body; the gas therein is also incompressible but, in general, of composition and temperature which are fixed but different from that in the outer layer. The flow in the inner layer is also rotational. * At the interface the radial velocity is zero; across the interface the pressure is continuous but the vorticity and tangential velocity are discontinuous.

The equations of motion for an axisymmetric, incompressible, rotational flow in spherical coordinates reduce to:

$$\frac{\partial}{\partial r}\left[r v_r \omega\right] + \frac{\partial}{\partial \varphi}\left[v_\varphi \omega\right] = 0 \qquad \text{(I-1)}$$

*The rotationality in the inner layer must be considered to be due to the shear stresses which actually occur between the inner and outer flows and which disappear in the idealization of the flow into two inviscid but rotational regions.

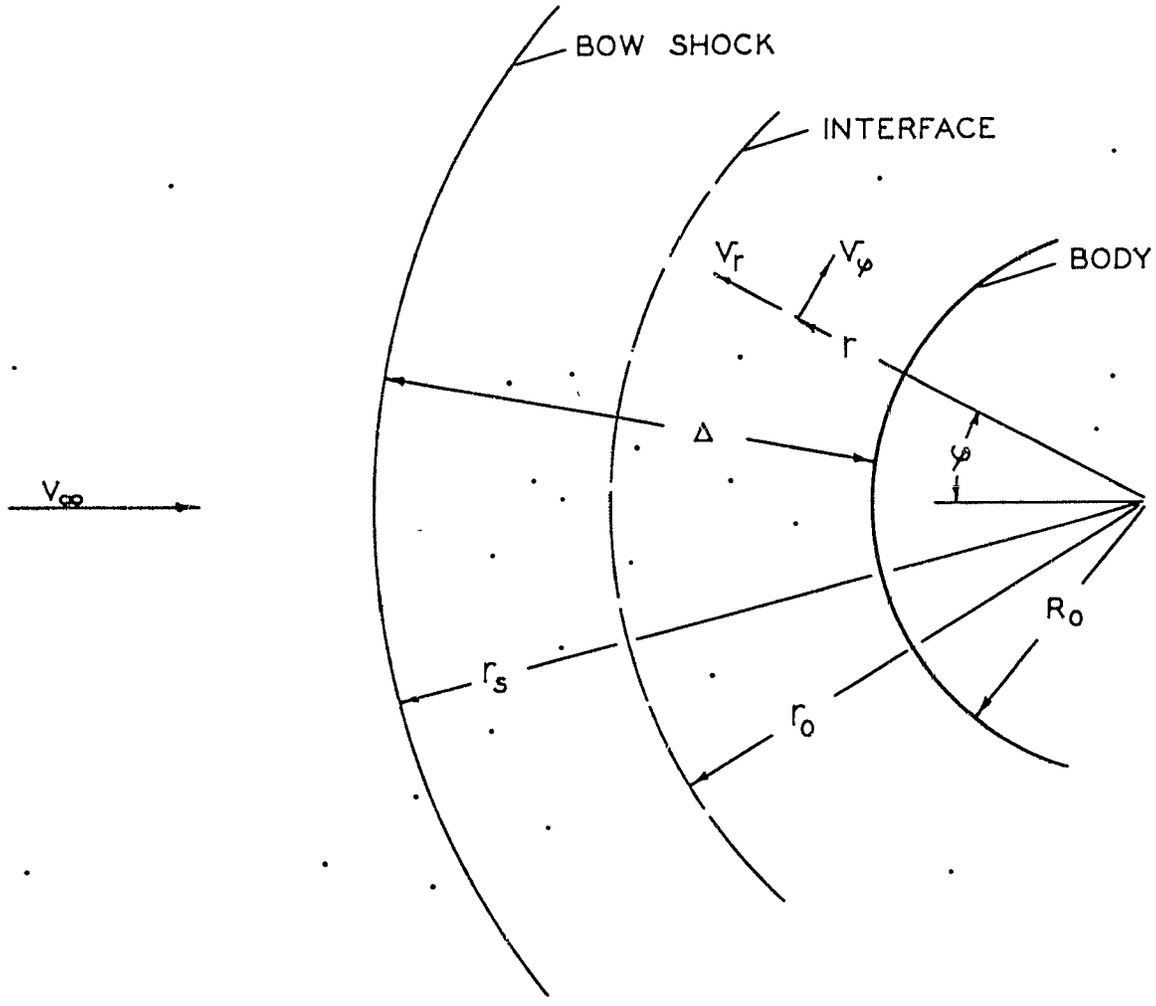

FIG. (12). COORDINATE SYSTEM USED IN THE DETERMINATION OF SHOCK STAND-OFF DISTANCE

Introduce the Stokes stream function, which satisfies mass continuity, and which is related to the radial and tangential velocity components by:

$$v_\varphi = \frac{1}{r \sin\varphi} \frac{\partial \psi}{\partial r} \tag{I-2}$$

$$v_r = -\frac{1}{r^2 \sin\varphi} \frac{\partial \psi}{\partial \varphi} \tag{I-3}$$

The vorticity in terms of the stream function is given by:

$$\omega = \frac{1}{r^3 \sin\varphi} \left[r^2 \frac{\partial^2 \psi}{\partial r^2} + \frac{\partial^2 \psi}{\partial \varphi^2} - \frac{\partial \psi}{\partial \varphi} \cot\varphi \right] \tag{I-4}$$

Outer Layer

Lighthill's solution applies for the layer between the spherical shock ($r=r_s$) and the interface ($r=r_o$). Accordingly, the velocity components at the outer surface of the interface are given by:

$$v_r = 0$$

$$v_\varphi = (v_\varphi)_e = \frac{V_\infty \sin\varphi}{2K} \left[(K-1)^2 (\bar{r}_s)^{-3} - K(K-4) \right] \tag{I-5}$$

where K is the static density ratio across a normal shock; i.e., ρ_e/ρ_∞, $\bar{r} = r/r_o$, and V_∞ is the free stream velocity. The location of the shock relative to the interface is determined by solving the following fifth degree algebraic equation for $\bar{r}_s \equiv r_s/r_o$.

$$2(K-6)(\bar{r}_s)^5 - \frac{5K(K-4)}{K-1} \bar{r}_s^2 + 3(K-1) = 0 \tag{I-6}$$

If there is no inner layer, i.e., no injection this equation with $r_o \to R_o$ gives the shock stand-off distance $\Delta/r_o = \Delta/R_o = \bar{r}_s - 1$.

Conditions at the interface

Now, applying the incompressible Bernoulli equation on both sides of the interface, and equating the static pressures all along the interface yields:

$$\frac{(v_\varphi)_e}{(v_\varphi)_c} = \left(\frac{\rho_c}{\rho_e}\right)^{\frac{1}{2}} = \left(\frac{W_c}{\theta_w W_e}\right)^{\frac{1}{2}} \tag{I-7}$$

where W_e = molecular weight of external fluid;
W_c = molecular weight of coolant fluid; and
θ_w = ratio of wall-to-stagnation temperature.

Combining Eqs. (I-5) and (I-7) provides two of the boundary conditions on the flow in the inner layer.

At $r = r_o$,

$$(v_\varphi)_c = \left[\frac{\theta_w W_e}{W_c}\right]^{\frac{1}{2}} \frac{V_\infty \sin\varphi}{2K} \left[(K-1)^2 (\bar{r}_s)^{-3} - K(K-4)\right] \tag{I-8}$$

$$v_r = 0 \tag{I-9}$$

If the body radius is denoted by R_o, the third boundary condition becomes

At $r = R_o$

$$v_\varphi = 0 \tag{I-10}$$

Inner layer

The solution of (I-1) satisfying the conditions (I-8) through (I-10) is of the form

$$\psi = \Psi(r) \sin^2\varphi \tag{I-11}$$

which upon substitution into Eq. (I-1) results in

$$r^3 \frac{d^3\Psi}{dr^3} - 2r^2 \frac{d^2\Psi}{dr^2} - 2r \frac{d\Psi}{dr} + 8\Psi = 0 \tag{I-12}$$

The solution of Eq. (I-12) with the proper boundary conditions is

$$\psi = \frac{\beta_c r_o^2}{3} \left\{ \bar{r}^2 - (\bar{r})^{-1} - \frac{[2+(\bar{R}_o)^{-3}][2(\bar{r})^{-1} - 5\bar{r}^2 + 3\bar{r}^4]}{12\bar{R}_o^2 - 10 - 2(\bar{R}_o)^{-3}} \right\} \tag{I-13}$$

where*

$$\beta_c = \frac{V_\infty}{2K}\left\{(K-1)^2(\bar{r}_s)^{-3} - K(K-4)\right\}\left[\frac{\theta_w W_e}{W_c}\right]^{\frac{1}{2}} \qquad (I-14)$$

and where $\bar{R} \equiv R_o/r_o$.

The radial velocity at the body surface can be determined from the stream function and is found to be:

$$(v_r)_w = \frac{2\beta_c}{3}\cos\varphi\left\{(\bar{R}_o)^{-3} - 1 + \frac{(2+\bar{R}_o^{-3})(2R_o^{-3} - 5 + 3\bar{R}_o^2)}{12\bar{R}_o^2 - 10 - 2\bar{R}_o^{-3}}\right\} \qquad (I-15)$$

It is noted that the solution corresponds to a non-uniform injection rate over the surface according to $\cos\varphi \simeq 1 - \varphi^2/2 + \ldots$.

The mass transfer rate of interest for comparison with experiment is obtained by integrating the injection velocity over the porous region and becomes:

$$m_c = \pi R_o^2 \rho_e\left[\frac{W_c}{\theta_w W_e}\right]^{\frac{1}{2}} \sin^2\varphi_i \frac{V_\infty}{3K}[(K-1)^2\bar{r}_s^{-3} - K(K-4)]$$

$$\left[(\bar{R}_o)^{-3} - 1 + \frac{(\bar{R}_o^{-3}+2)(2\bar{R}_o^{-3} - 5 + 3\bar{R}_o^2)}{12\bar{R}_o^2 - 10 - 2\bar{R}_o^{-3}}\right] \qquad (I-16)$$

Utilizing strong shock conditions, the free stream velocity (V_∞) can be related to stagnation conditions behind the normal shock and the density ratio (K) by,

$$V_\infty^2 = \frac{Kp_{s_e}}{\rho_{s_e}} \qquad (I-17)$$

---

*It should be noted that β_c is the stagnation point velocity gradient $dv\varphi/d\varphi]_c$ at the interface. If the velocity gradient of the external flow (at the interface is denoted by β_e, the relation between the two gradients across the interface is given by: $\beta_c = \beta_e\left[\frac{\theta_w W_e}{W_c}\right]^{\frac{1}{2}}$.

There results the non-dimensional similarity parameter, N_s given by:

$$N_s = \frac{m_c}{R_o^2(\rho_{s_e}\mu_{s_e})^{\frac{1}{2}}}\left[\frac{\theta_w W_e}{W_c}\right]^{\frac{1}{2}} = \frac{\pi}{3K^{\frac{1}{2}}}\sin^2\varphi_i\left[(K-1)^2\bar{r}_s^{-2} - K(K-4)\right]$$

$$\left[\bar{R}_o^3 - 1 + \frac{(\bar{R}_o^{-3}+2)(2\bar{R}_o^{-3} - 5 + 3\bar{R}_o^2)}{12\bar{R}_o^2 - 10 - 2\bar{R}_o^{-3}}\right] \qquad (I-18)$$

Consider the application of this analysis to a particular example. If M_∞ and the other free stream quantities are known, K is determined by normal shock conditions. The parameter N_s and the angle φ_i are assumed known. Now Eq. (I-6) can be solved for $\bar{r}_s$ and Eq. (I-18) can then be solved for R_o. Note that $\Delta/R_o = (r_s/R_o) - 1 = (\bar{r}_s/\bar{R}_o - 1$. In Figure 6 the variation of Δ/R_o with N_s for $M_\infty = 8.0$ has been given and compared to experiment.

Since the stagnation enthalpy achieved in the wind tunnel is much less than that corresponding to free flight conditions at $M_\infty = 8.0$, the strong shock approximations are not strictly valid for the analysis of the experimental data. As a result, in computing the theoretical curve presented in Figure 6, the approximation attendant with Eq. (I-17) was not used so that Eq. (I-18) was modified somewhat.

Tangential velocity distribution

It is further of interest to consider the variation of the tangential velocity distribution with N_s and shown in Figure 13. It is noted that for relatively small values of N_s the ratio $(r_o/R_o) \simeq 1$, and the tangential velocity distribution is close to linear; thus the inviscid model for the stagnation point boundary layer gives in this case the same tangential velocity distribution as the boundary layer calculations which were given in reference 2 and which were based on $\delta/R_o << 1$. However, for increasing N_s, the ratio r_o/R_o increases and sphericity results in a nonlinear distribution of tangential velocity. Presumably, the boundary layer equations with $\delta/R_o \simeq 1$ would result in a similar distribution except in a relatively thin region which is close to the outer edge and which involves significant shear stresses.

In the outer flow layer, with the assumption of a spherical shock, the ratio of vorticity to distance from the center line is constant throughout the region. For the boundary conditions utilized in the solution of the inner flow layer, it is noted that this ratio is also constant in this flow region.

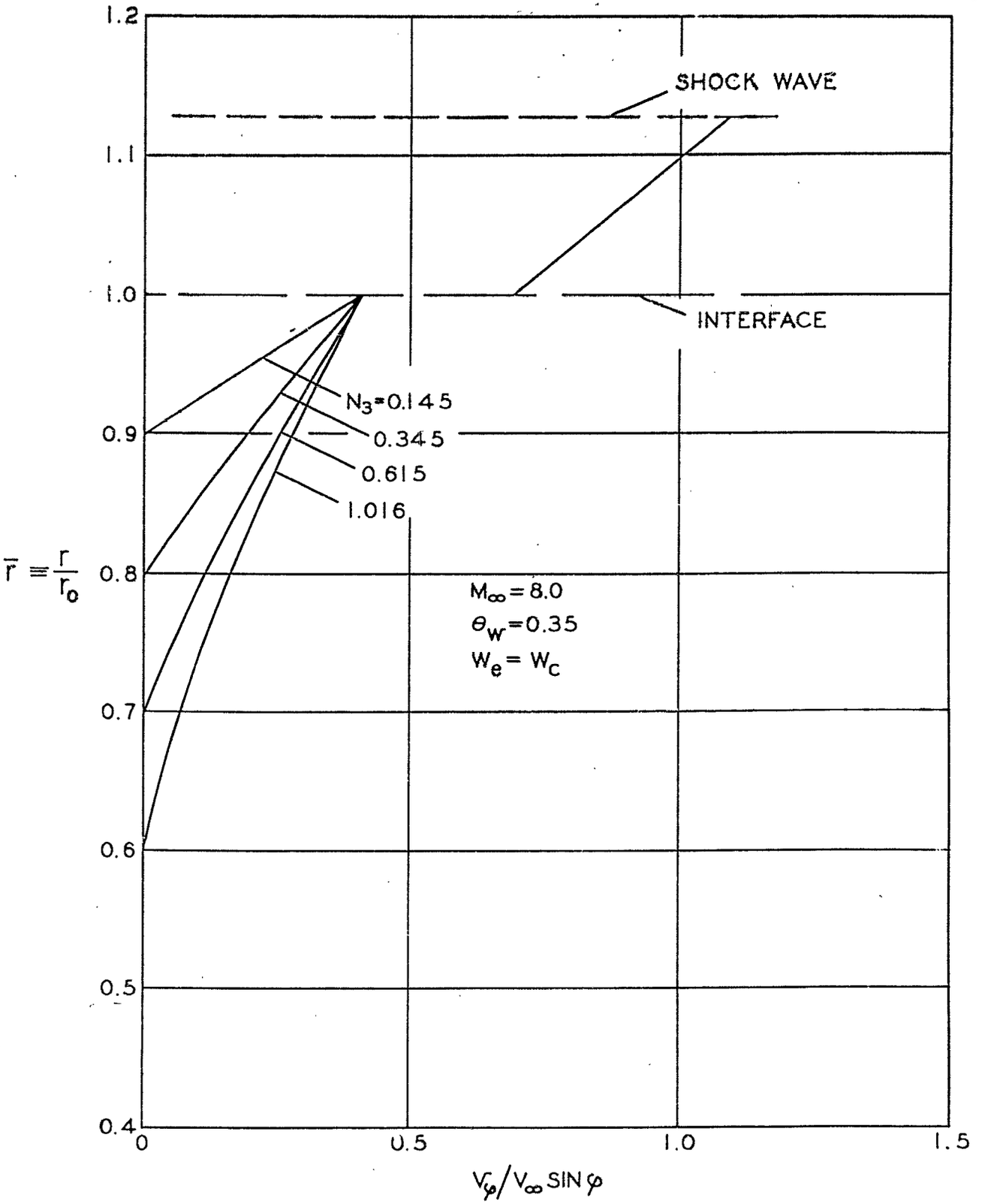

FIG. (13) TANGENTIAL VELOCITY PROFILES FOR VARIOUS MASS TRANSFER RATES (NITROGEN)

Empirical correction for velocity gradient

It is well known that the velocity gradient β_e is not well predicted by the Lighthill theory, the error being due to the assumed spherical shock wave. An empirical correction to the analysis presented here can, however, be made; if β_e is computed from Newtonian theory applied at the interface, then Eq. (I-18) becomes

$$N_s = \frac{2\pi\sqrt{2}}{3} \sin^2 \varphi_i \left\{ (\bar{R}_o)^{-3} - 1 + \frac{(2 + \bar{R}_o^{-3})(2\bar{R}_o^{-3} - 5 + 3\bar{R}_o^{3})}{12\bar{R}_o^{3} - 10 - 2\bar{R}_o^{-3}} \right\} \quad \text{(I-18a)}$$

For $M_\infty = 8.0$ the results of the determination of Δ/R_o from Eq. (I-18a) are also shown in Figure 6 and are seen to be in somewhat better agreement with experiment.